Research

New Phytologist

Light acclimation interacts with thylakoid ion transport to govern the dynamics of photosynthesis in Arabidopsis

Thekla von Bismarck[1], Kübra Korkmaz[1], Jeremy Ruß[1], Kira Skurk[1], Elias Kaiser[1], Viviana Correa Galvis[1], Jeffrey A. Cruz[2,3], Deserah D. Strand[1], Karin Köhl[1], Jürgen Eirich[4], Iris Finkemeier[4], Peter Jahns[5], David M. Kramer[2,3] and Ute Armbruster[1]

[1]Max Planck Institute of Molecular Plant Physiology, 14476, Potsdam, Germany; [2]DOE-Plant Research Laboratory, Michigan State University, East Lansing, MI 48824, USA; [3]Department of Biochemistry and Molecular Biology, Michigan State University, East Lansing, MI 48824, USA; [4]Plant Physiology, Institute of Plant Biology and Biotechnology, University of Münster, 48149, Münster, Germany; [5]Plant Biochemistry, Heinrich-Heine-University Düsseldorf, 40225, Düsseldorf, Germany

Authors for correspondence:
Ute Armbruster
Email: armbruster@mpimp-golm.mpg.de

David M. Kramer
Email: kramerd8@msu.edu

Received: *16 February 2022*
Accepted: *27 September 2022*

New Phytologist (2023) **237:** 160–176
doi: 10.1111/nph.18534

Key words: *Arabidopsis thaliana*, dynamic photosynthesis, light acclimation, nonphotochemical quenching, thylakoid ion transport, zeaxanthin.

Summary

- Understanding photosynthesis in natural, dynamic light environments requires knowledge of long-term acclimation, short-term responses, and their mechanistic interactions. To approach the latter, we systematically determined and characterized light-environmental effects on thylakoid ion transport-mediated short-term responses during light fluctuations.
- For this, *Arabidopsis thaliana* wild-type and mutants of the Cl^- channel VCCN1 and the K^+ exchange antiporter KEA3 were grown under eight different light environments and characterized for photosynthesis-associated parameters and factors in steady state and during light fluctuations. For a detailed characterization of selected light conditions, we monitored ion flux dynamics at unprecedented high temporal resolution by a modified spectroscopy approach.
- Our analyses reveal that daily light intensity sculpts photosynthetic capacity as a main acclimatory driver with positive and negative effects on the function of KEA3 and VCCN1 during high-light phases, respectively. Fluctuations in light intensity boost the accumulation of the photoprotective pigment zeaxanthin (Zx). We show that KEA3 suppresses Zx accumulation during the day, which together with its direct proton transport activity accelerates photosynthetic transition to lower light intensities.
- In summary, both light-environment factors, intensity and variability, modulate the function of thylakoid ion transport in dynamic photosynthesis with distinct effects on lumen pH, Zx accumulation, photoprotection, and photosynthetic efficiency.

Introduction

Plants provide us with food and renewable energy. This involves the process of photosynthesis, which uses light energy to fix CO_2 and drive plant metabolism. In crop canopies, light availability for photosynthesis can fluctuate immensely (Kaiser *et al.*, 2017). Our current knowledge of photosynthesis under natural dynamic light conditions may pose a limitation for strategies to increase plant production in the field (Kaiser *et al.*, 2019; Long *et al.*, 2022). Mechanistic understanding is needed on at least two different timescales: long-term acclimation to natural dynamic light environments and short-term responses to changes in light intensity. Extremely little is known about how both responses interact.

For the model plant *Arabidopsis thaliana* (Arabidopsis), it has been shown that light acclimation involves upregulation of photosynthetic capacity with light intensity (Walters & Horton, 1994, 1995; Bailey *et al.*, 2001, 2004; Athanasiou *et al.*, 2009; Alter *et al.*, 2012; Mishra *et al.*, 2012; Schumann *et al.*, 2017; Vialet-Chabrand *et al.*, 2017; Flannery *et al.*, 2021) and natural environment acclimation increases photoprotective capacity (Mishra *et al.*, 2012; Schumann *et al.*, 2017; Pescheck & Bilger, 2019).

Plants can dissipate absorbed light energy as heat via nonphotochemical quenching (NPQ). Nonphotochemical quenching provides a short-term regulatory mechanism that is required for fitness in the field (Külheim *et al.*, 2002). Energy-dependent NPQ (qE) is the main and most rapid NPQ component in plants. The qE responds to the proton concentration of the lumen (Briantais *et al.*, 1979; Niyogi, 1998; Li *et al.*, 2000, 2004) and deactivates within seconds (Demmig-Adams *et al.*, 1996). Upon protonation, the PsbS protein catalyzes a rearrangement of the photosystem (PS) II supercomplex, which is required for qE activation (Johnson *et al.*, 2011). The pigment zeaxanthin (Zx) plays an additional role in qE. Zeaxanthin is synthesized from the epoxidated xanthophyll violaxanthin (Vx) by the lumen-localized violaxanthin de-epoxidase (VDE) that is also activated by protonation (Li *et al.*, 2004; Arnoux *et al.*, 2009). The Zx levels respond to lumen pH on the minute timescale (Hager, 1969; Demmig *et al.*, 1987; Hartel *et al.*, 1996;

Niyogi, 1998). Recent data point toward a function of Zx in regulating qE dynamics rather than the dissipation process itself (Holt *et al.*, 2005; Johnson *et al.*, 2009; Nilkens *et al.*, 2010; Xu *et al.*, 2015; Sacharz *et al.*, 2017; Tutkus *et al.*, 2019).

The light reactions in the thylakoid membrane lead to an accumulation of protons in the lumen, forming the proton motive force (pmf). The pmf is composed of a membrane potential ($\Delta\psi$) and the proton concentration gradient (ΔpH). $\Delta\psi$ and ΔpH fuel adenosine triphosphate (ATP) synthesis from adenosine diphosphate (ADP) and inorganic phosphate by driving protons through the ATP synthase (Mitchell, 1966). When light intensity increases, qE is activated, because rates of proton influx into the lumen transiently become higher than efflux via the ATP synthase. qE activation is further facilitated by $\Delta\psi$ dissipation through counter ion flux, which shifts pmf composition toward higher ΔpH (Vredenberg, 1969; Van Kooten *et al.*, 1986; Cruz *et al.*, 2001). The high $\Delta\psi$-activated Cl^- channel VCCN1 was shown to participate in $\Delta\psi$ dissipation and accelerate qE induction (Duan *et al.*, 2016; Herdean *et al.*, 2016; Dukic *et al.*, 2019). The qE is rapidly switched off in low light through the dissipation of ΔpH by a proton exchange mechanism (Armbruster *et al.*, 2014). Proton export from the lumen by the thylakoid localized K^+ exchange antiporter 3 (KEA3) changes pmf composition toward higher $\Delta\psi$ without large effects on pmf size (Armbruster *et al.*, 2014; Kunz *et al.*, 2014). KEA3 activates after the transition to photosynthesis-limiting light conditions, thereby accelerating qE relaxation and increasing photosynthetic light use efficiency (Armbruster *et al.*, 2014, 2016). Under excess light, KEA3 inactivates via its C-terminus (Armbruster *et al.*, 2016; Uflewski *et al.*, 2021). The inhibition of KEA3 is required for high qE, protecting the photosystems from photodamage in excess light (Uflewski *et al.*, 2021).

By rapidly adjusting the composition of the pmf and thus lumen pH during light transients, ion transport mechanisms have been proposed to speed up the synchronization of photosynthetic light reactions with downstream metabolism via changing qE (Li *et al.*, 2021; Uflewski *et al.*, 2021). In the present study, we systematically addressed how long-term acclimation to different light intensities and patterns affects dynamic photosynthesis. Thereby, we found that light-environmental factors interact with the function of the two known thylakoid ion transport proteins VCCN1 and KEA3. Further mechanistic understanding was gained by a modified spectroscopy approach that allowed high temporal resolution of qE and $\Delta\psi$ dynamics.

Materials and Methods

Plant material and growth

Arabidopsis (*A. thaliana* (L.) Heynh.) plants were grown in 6-cm pots on MPG horticultural substrate (Stender, Schermbeck, Germany with 1 g l^{-1} Osmocote start) in phytochambers (BBC York, Mannheim, Germany) with a 12-h light period, and temperatures/relative humidity set to 20°C/60% in the light and 16°C/75% in the dark, under six different light conditions from seed to mature rosette. Details on light treatments can be found in Figs 1(a), S1, and Table S1. For natural day (ND) experiments, plants were grown in 13-cm pots in a polytunnel at the Max Planck Institute of Molecular Plant Physiology (coordinates: 52°24′55.44″N, 12°58′7.464″E). After 3 wk of pre-cultivation in a phytotron (120 µmol photons m^{-2} s^{-1}, climate conditions as described above), plants were grown in the polytunnel from 21 March to 28 March 2019 (ND_1) or 4 April to 14 April 2019 (ND_2, Figs 1a, S1a). Measurements were performed on Days 7–8 (ND_1) or 8–9 (ND_2) after transfer and on mature phytotron-grown plants (FD_L: 5–6 wk, FD_M: 4–5 wk FD_H: 3–4 wk, DD_S: 3–4 wk, DD_F: 5–6 wk, DD_{SF}: 4–5 wk) 1–2 wk before bolting of wild-type Columbia-0 (WT) and mutants: *vccn1-1*: Salk 103612; *vccn1-2*: Gabi-Kat 796C09, *kea3-1*: Gabi-Kat 170G09; *kea3-2*: Sail 556_E12, *npq2*: Salk_059469, *npq2 kea3* (Armbruster *et al.*, 2014; Duan *et al.*, 2016; Herdean *et al.*, 2016) and *npq4* (Niyogi, 1998). *npq2* and *npq2 kea3-1* together with controls were grown under elevated humidity using a dome. Rosette dry weights at indicated times after sowing were determined after oven-drying (75°C, 7 d). PFD_{mean} represents the average light intensity and PFD_{var}, the sum of light intensity, changes over the day (Table S1).

Spectroscopic analyses

For Chl*a* fluorescence analyses, the Maxi Imaging-PAM (Walz GmbH, Effeltrich, Germany) or an integrated diode emitter array spectrophotometer/fluorometer (IDEAspec, Hall *et al.*, 2013) was used on whole rosettes or section of a fully expanded leaf, respectively. Saturation light pulses were applied after 30-min dark treatment to determine F_m and during illumination with actinic light for F_m'. Nonphotochemical quenching was calculated as $(F_m - F_m')/F_m'$, Φ_{PSII} as $(F_m' - F')/F_m'$, and F_v/F_m as $(F_m - F_0)/F_m$ (reviewed by Baker, 2008). For light fluctuations, four iterations of 4-min low irradiance (LI, 90 µmol photons m^{-2} s^{-1}) and 1-min high irradiance (HI; 900 µmol photons m^{-2} s^{-1}) were applied; then, a final 4-min LI phase followed by 5-min darkness. The first three fluctuations showed strong differences between photosynthetic parameters. The third and fourth fluctuations were comparable. Thus, the third fluctuation was characterized.

Absorbance changes were measured at six wavelengths (475, 488, 505, 520, 535, and 545 nm) near-simultaneously on the IDEAspec separated by 1-ms intervals and recorded every 30 ms. Measuring light was supplied by red LEDs (655 nm, bandpass *c.* 20 nm; Hall *et al.*, 2013). Normalized relative extinction coefficients for electrochromic shift (ECS), qE, Zx and drift at wavelengths λ were derived according to published literature (Bilger *et al.*, 1989; Niyogi, 1998; Li *et al.*, 2000; Sacksteder *et al.*, 2000, 2001; Golding *et al.*, 2005). The deconvolution equation and additional information can be found in Table S2.

Absorbance measurements were performed under the same light fluctuations as Chl*a* fluorescence measurements with the addition of a 30-s dark phase following every HI to LI transition after 20 s. Accordingly, plants were exposed to 4-min LI, and then, four iterations of 60-s HI, 20-s LI, 30-s darkness, and 220-s LI. Electrochromic shift and qE_{535} traces were

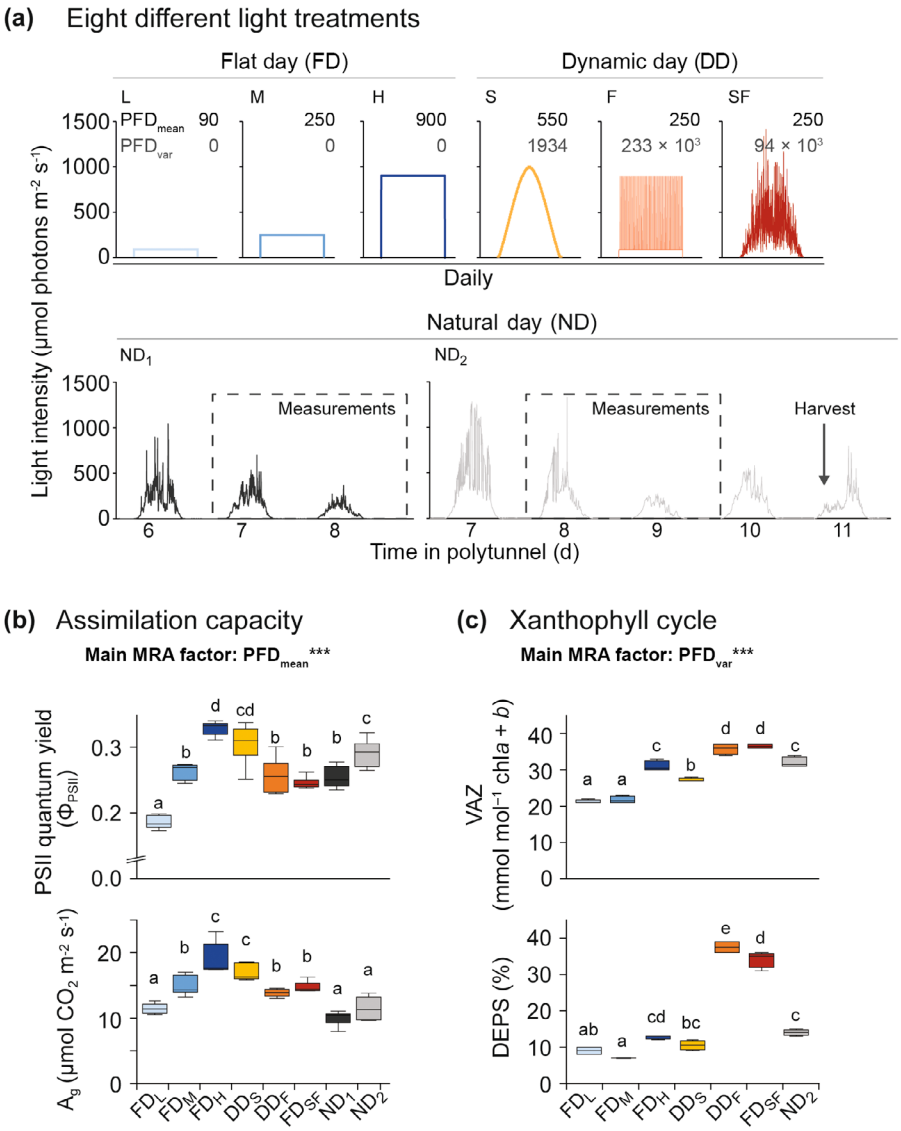

Fig. 1 Environmental acclimation adjusts steady-state photosynthesis and thylakoid pigment composition. (a) *Arabidopsis thaliana* wild-type (WT) was grown in 12 h : 12 h, light : dark cycles under constant growth light (flat day, FD) at indicated intensities (low, FD_L; medium, FD_M; and high, FD_H), dynamic growth light (dynamic day, DD) with varying degrees of light fluctuations (sinusoidal, DD_S; step-wise fluctuating, DD_F; sinusoidal with random light fluctuations, DD_{SF}) or natural growth conditions in a polytunnel (natural day; ND_1 and ND_2). Humidity and temperature, as well as light spectra, can be found in Fig. S1. Average and variable photon flux densities (PFD_{mean} and PFD_{var}, respectively) are displayed (see Fig. S1; Table S1 for additional information). (b) PSII quantum efficiency (Φ_{PSII}, upper panel) at 700 µmol photons m^{-2} s^{-1} and gross assimilation rate (A_g, lower panel) at 900 µmol photons m^{-2} s^{-1} correlate positively with PFD_{mean} as the main factor as determined by multiple regression analysis (MRA). PFD_{mean} for ND was set as average of 3 d before the measurement. Averages of $n = 5–7 \pm$ SE are shown. (c) Levels of photoprotective xanthophylls (VAZ, sum of violaxanthin, antheraxanthin, zeaxanthin, and upper panel) and their de-epoxidation state (DEPS, lower panel) correlate positively with PFD_{var} as the main factor. Averages of $n = 4 \pm$ SE are shown. Thylakoid pigment content can be found in Table S3. For thylakoid isolation, plants were removed from the growth chamber at 2 h after start of the light period and harvest of whole rosettes was performed in the laboratory at room light. (b, c) The middle line and the lower and upper boundaries of the box represent the median and the 25th and 75th percentile, respectively. Whiskers extend to the maximum and minimum. An ANCOVA was used to determine the effects of PFD_{mean} and PFD_{var} on the displayed parameters. The main factor is indicated on top of the panels with ***, $P < 0.0001$. Different lower case letters indicate significant differences between the light treatments. Statistical analyses can be found in Table S6.

drift-corrected using the last 15 s of the dark phase and 10 s of the LI just before the HI transition, respectively. $\Delta\psi$ and ΔpH were calculated from the multiphasic ECS kinetics during the 30-s dark interval (Cruz *et al.*, 2001; Takizawa *et al.*, 2007). Total light-induced pmf (ECS_t) and trans-thylakoid proton conductivity of ATP synthase (g_{H^+}) were calculated from relaxation kinetics at 520 nm during a 500 ms dark interval (Kanazawa & Kramer, 2002). Because of the low signal-to-noise ratio at 520 nm in LI, ECS_t and g_{H^+} were averaged between the third and fourth fluctuation.

Gas exchange measurements used the Li-Cor 6400 gas exchange system (Li-Cor Biosciences, Lincoln, NE, USA; flow rate: 500 µmol s^{-1}, CO_2 concentration: 400 µmol mol^{-1}, and humidity: 60%) coupled to the Maxi Imaging-PAM on whole

plants, or the GFS-3000 open gas exchange system with LED array 3056-FL (Walz GmbH; flow: 600 µmol s^{-1}, CO_2 concentration: 400 µmol mol^{-1}, humidity: 60%) on the youngest fully developed leaf in a custom-made 3 × 1 cm cuvette. Plants were dark-acclimated for 30 min, inserted into the cuvette, and then exposed to 10 min of 900, 10 min of 90 µmol m^{-2} s^{-1}, and 5 min of darkness. CO_2 assimilation rate was normalized on leaf area. Net assimilation rates (A_n) and dark respiration (R_d) were averaged over the final 30 s of the light or subsequent dark phase, respectively. Gross assimilation rate (A_g) was calculated as $A_n + R_d$.

All spectroscopic measurements were performed continuously between 2 and 10 h into the photoperiod by repeating a fixed sequence of different genotypes.

Quantification of photosynthetic proteins and pigments

Wild-type plants for total protein and thylakoid isolations were removed from the growth chamber 2 h into the light period. Harvest of whole rosettes was performed in the laboratory at room light. Total protein was extracted from ground tissue by incubating 20 mg with 200 µl protein extraction buffer (200-mM Tris, pH 6.8, 8% (w/v) SDS, 40% (v/v) glycerol, and 200-mM DTT) at 65°C for 10 min (Armbruster *et al.*, 2016). Proteins were separated on SDS-PAGEs, blotted onto nitrocellulose, visualized with Ponceau Red (0.1% (w/v) Ponceau S in 5% (v/v) acetic acid, for Rubisco quantification) and detected with antibodies specific for KEA3 (Armbruster *et al.*, 2014), Lhcb3 (AS01002), PsbD (AS06146), PetA (AS08306), PsaA (AS06172), AtpB (AS05085; all Agrisera, Vännäs, Sweden), and Actin (A0480; Sigma-Aldrich; all diluted according to the manufacturer's instructions). Signal intensities were quantified by ImageJ, normalized to FD_M, and corrected for loading by actin from the same blot.

Thylakoids were isolated from WT rosettes (Armbruster *et al.*, 2014) and used for quantifying pigment content and thylakoid complex composition. For the latter, proteins were extracted and digested with trypsin (Morgan *et al.*, 2008). Sample processing and LC–MS/MS data acquisition settings and raw data processing were performed as described (Lassowskat *et al.*, 2017; Uflewski *et al.*, 2021) with the following adjustments: peptides were purified using SDP-RPS stage tips (Kulak *et al.*, 2014) before LC–MS analysis. MaxQuant 1.6.17.0 (Cox & Mann, 2008) was used with default settings. Match between runs and intensity-based absolute quantification (iBAQ) were additionally enabled (Lassowskat *et al.*, 2017; Uflewski *et al.*, 2021). The iBAQ data were used for quantification to compensate for contaminators during thylakoid preparation according to Flannery *et al.* (2021).

For the quantification of leaf pigments and KEA3 content from the different genotypes, entire rosettes were plunged into liquid N_2 before the start of or 6 h into the light period. Pigments were extracted from 20 mg of ground leaf powder or from thylakoid membranes, isolated as described in the previous section, corresponding to 20 µg of chlorophyll by addition of 100% acetone on ice and in the dark. The pigment extracts were analyzed according to Färber *et al.* (1997).

Statistics and clustering

Normality distribution and equal variance were analyzed by ANOVA followed by Tukey's test. In case of failed normality and/or equal variance, ANOVA on ranks was carried out, followed by Student–Newman–Keuls (SNK) or Dunn's test. One-way ANCOVA was performed using Sas 9.4 (SAS Institute, Cary, NC, USA) with growth conditions as class variables and PFD_{mean} and PFD_{var} as covariates. Multiple regression analysis (MRA) was performed using either Sas, SigmaPlot 14.5, or Python 3.7.4 (scikit-learn). Correlation analysis was performed using Python 3.7.4 (scipy) or SigmaPlot, employing Pearson's or Spearman's rank correlation for linear or monotonic relationships, respectively. *K*-mean clustering was performed on log_2 transformed, normalized NPQ (mutant/WT) in Python (seaborn).

Results

Growth light intensity and fluctuations have distinct effects on photosynthetic capacity and pigment composition

We grew *A. thaliana* (Arabidopsis) under different light treatments in climate-controlled phytotrons and a polytunnel under natural light and climate (Figs 1a, S1; Table S1). Steady-state photosynthesis and composition of the thylakoid membrane were determined from WT (Tables S3–S5). Results were analyzed by MRA using two light variables as covariates: fluctuations in light intensity, quantified as the sum of light intensity changes over 1 d (variable photon flux density, PFD_{var}); and, the mean daily intensity (mean photon flux density, PFD_{mean}, Tables S6, S7). The results revealed PFD_{mean} as the predominant light factor that could explain differences in the quantum efficiency of photosystem II (Φ_{PSII}) and gross CO_2 assimilation rate (A_g) at high irradiance (HI; Figs 1b, S2). Levels and de-epoxidation state of the xanthophyll-cycle pigments violaxanthin, antheraxanthin, and zeaxanthin (VAZ) correlated most strongly with PFD_{var} (Figs 1c, S2).

Further small PFD_{mean} effects were found on the levels of PSII and the light-harvesting complex (LHC) of PSII (LHCII), which correlated positively and negatively with PFD_{mean}, respectively (Fig. S3). A positive correlation of the photosystem reaction center (RC) : LHC ratio with PFD_{mean} was supported by levels of RC-bound β-carotene and Chl*a*/*b* ratio rising with PFD_{mean} (Chl*b* is only present in LHCs and not in RCs; Thornber & Highkin, 1974). Additional small PFD_{var} effects were found on the levels of Cyt b_6f complex, ATP synthase, and Chl*a*/*b*, which correlated positively, and LHCII and PSI, which correlated negatively (Fig. S3).

Our results from characterizing light acclimation effects on photosynthesis are in line with previous smaller scale analyses (Bailey *et al.*, 2004; Alter *et al.*, 2012; Schumann *et al.*, 2017; Vialet-Chabrand *et al.*, 2017; Matthews *et al.*, 2018; Pescheck & Bilger, 2019): We show that PFD_{mean} is a main determinant of Φ_{PSII} and A_g, which confirms that growth light intensity sculpts photosynthetic capacity. Additionally, we show that levels of de-

New Phytologist

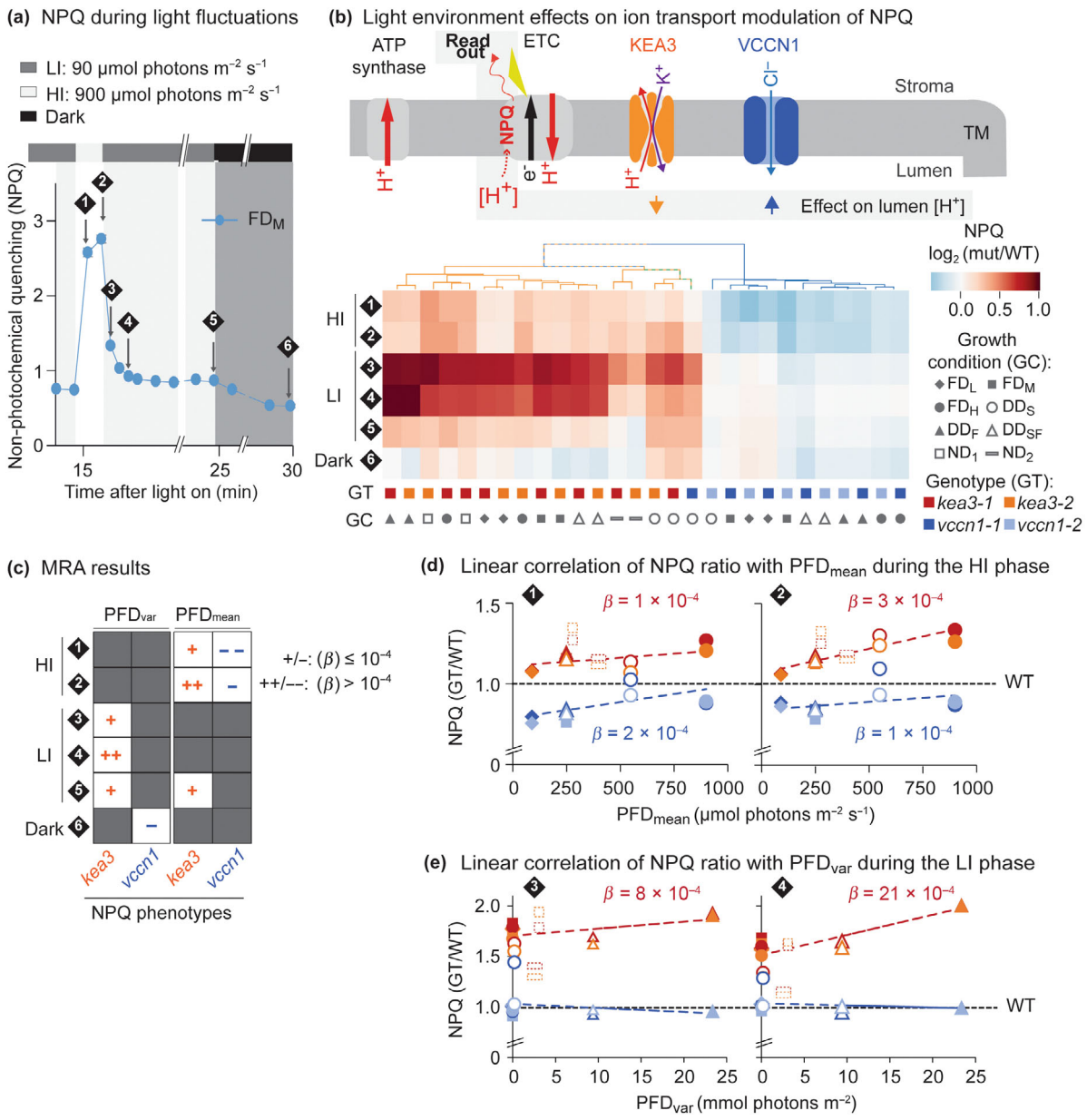

Fig. 2 Light acclimation interacts with the functions of KEA3 and VCCN1 in nonphotochemical quenching (NPQ) dynamics. (a) Chla fluorescence was measured in dark-acclimated *Arabidopsis thaliana* wild-type (WT) and two mutant alleles each of *kea3* and *vccn1*, grown under eight different light environments (FD, flat day: FD_L – low, FD_M – medium, FD_H – high; DD, dynamic day: DD_S – sinusoidal, DD_F – fluctuating, DD_{SF} – sinusoidal fluctuating; and ND, natural day), during four iterations of 4-min low irradiance (LI, 90 µmol photons m^{-2} s^{-1}) and 1-min high irradiance (HI, 900 µmol photons m^{-2} s^{-1}), a final 4-min LI phase followed by 5-min darkness. Measurements were performed continuously between 2 and 10 h into the photoperiod by repeating a fixed sequence of different genotypes. Nonphotochemical quenching (NPQ) was calculated for all growth light conditions and complete traces can be found in Fig. S5. Average of $n = 6 \pm$ SE is shown for NPQ of WT grown under FD_M during the third fluctuation, end of the final LI, as well as of the dark phase. (b) Scheme of the electron transport chain (ETC), the adenosine triphosphate synthase, the VCCN1 Cl^- channel, and the KEA3 H^+/K^+ antiporter located in the thylakoid membrane (TM). Nonphotochemical quenching of the mutants as compared to WT serves as readout for the activity of KEA3 and VCCN1 during light fluctuations and their effects on the proton concentration of the lumen. *K*-mean clustering of log_2 transformed NPQ ratios (mutant/WT) at six different time points (shown in (a)) is presented as a heatmap. Average NPQ values of $n = 5$–7 were used for the analysis. (c) Multiple regression analyses were performed on mutant/WT NPQ ratios at indicated time points (shown in a) using average and variable photon flux densities (PFD_{mean} and PFD_{var}, respectively) as covariates. Significant effects on the mutant NPQ phenotype compared with WT are indicated by plus and minus signs (+, deviating from, and −, approaching WT with increasing light factor; *vccn1*, blue; *kea3*, red). Number of signs denotes the slope (β) determined by the MRA analysis as an indicator for the amplitude of the effects by PFD_{mean} and PFD_{var} on NPQ as displayed in the figure. The complete statistical analyses can be found in Table S8. (d, e) Nonphotochemical quenching ratio of mutant/WT at indicated timepoints (30 and 60 s after LI to HI shift, d, or 20 and 60 s after HI to LI shift), (e) plotted as a function of PFD_{mean} (d) or PFD_{var} (e) with red or blue broken lines representing the linear fits through mutant/WT NPQ ratios of *kea3* or *vccn1*, respectively, and corresponding slopes (β). (a, d, e) Note that some error bars are smaller than data point symbols and therefore not visible.

epoxidized xanthophyll-cycle pigments, which have a photoprotective function, correlate positively with PFD_{var}. This finding supports the upregulation of photoprotective mechanisms in fluctuating growth light environments.

Thylakoid ion transport shapes dynamic NPQ in a light-environment-dependent manner

Two mutant alleles each of *kea3* and *vccn1* were grown alongside WT under different light environments. All mutants visually resembled WT and showed comparable maximum PSII quantum efficiency (F_v/F_m) under each growth condition (Fig. S4). We determined the effects of environmental acclimation on the function of VCCN1 as an accelerator of qE induction (Duan *et al.*, 2016; Herdean *et al.*, 2016) and KEA3 as an accelerator of qE relaxation (Armbruster *et al.*, 2014). For this, we exposed plants to a short, 10-fold fluctuation in light intensity between 90 (low irradiation, LI) and 900 µmol photons m^{-2} s^{-1} (high irradiation, HI, 1 min) and determined NPQ from Chl*a* fluorescence analyses (Figs 2a,b, S5). In previous reports on *kea3* and *vccn1*, plants had always been grown under low light intensities. Mutant phenotypes for FD_L were as previously published: *vccn1* induced NPQ more slowly in HI (Duan *et al.*, 2016; Herdean *et al.*, 2016), and *kea3* showed delayed NPQ relaxation in LI (Armbruster *et al.*, 2014, 2016; Fig. S5). For a systematic comparison of growth light effects on mutant NPQ phenotypes, the NPQ ratios of mutant/WT were calculated for six time points during the light fluctuation (Fig. 2a). The NPQ ratios were *K*-mean clustered and analyzed by MRA using PFD_{mean} and PFD_{var} as covariates. The clustered heatmap in Fig. 2(b) shows two main groups. One contains only *vccn1* and is characterized by NPQ reduction during the HI phase. The second group is dominated by *kea3* (containing *vccn1-1* in DD_S) and characterized by elevated NPQ most strongly during the LI, but also in

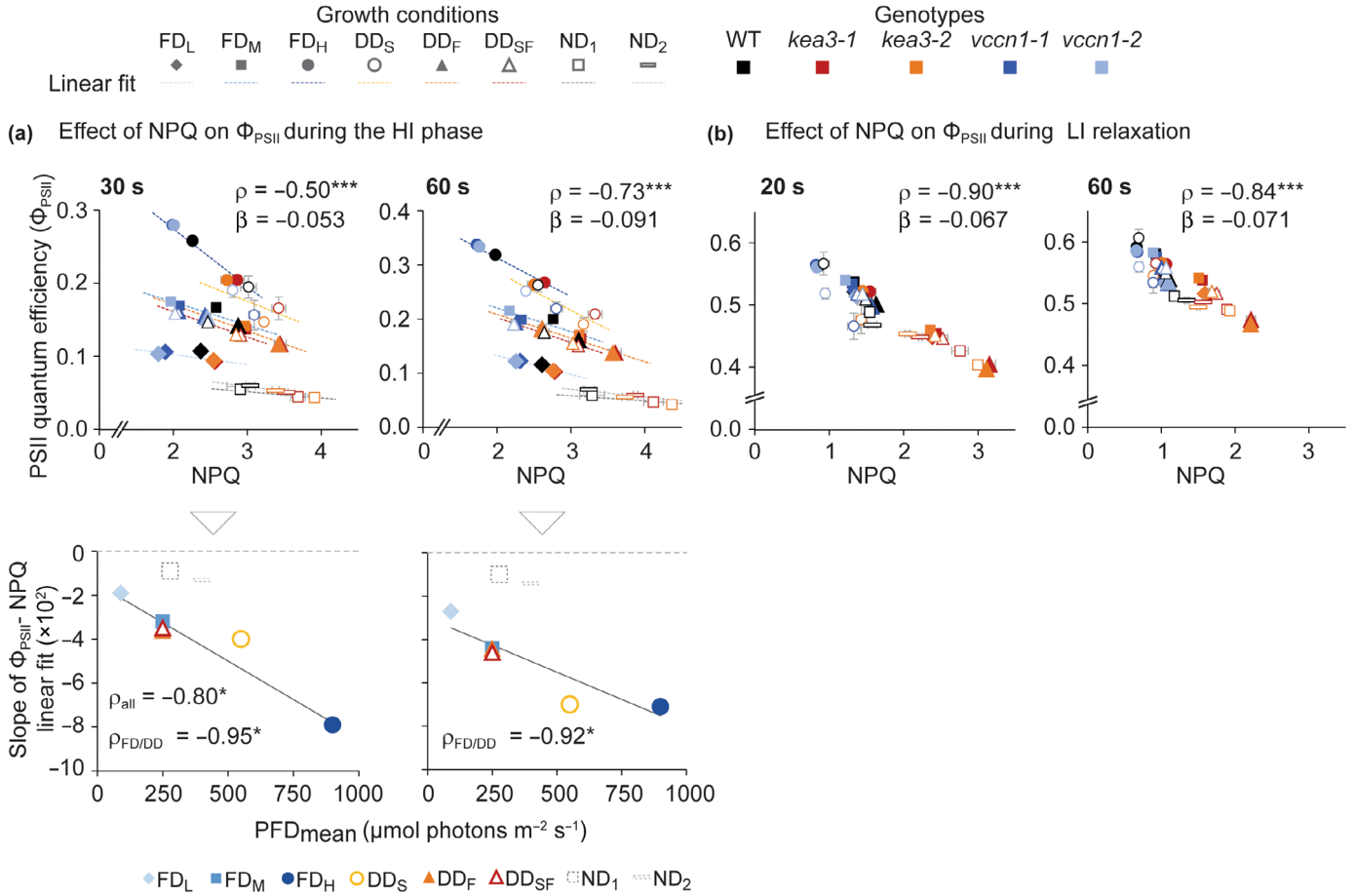

Fig. 3 Growth light intensity determines the effect of thylakoid ion transport on photosynthetic efficiency. (a) Upper panels: PSII quantum efficiency (Φ_{PSII}) at 30 or 60 s after transfer from low irradiance (LI, 90 µmol photons m^{-2} s^{-1}) to high irradiance (HI, 900 µmol photons m^{-2} s^{-1}, as in Fig. 2) was plotted against nonphotochemical quenching (NPQ) of *Arabidopsis thaliana* wild-type (WT), *kea3*, and *vccn1* from eight different growth conditions (FD, flat day: FD_L – low, FD_M – medium, FD_H – high; DD, dynamic day: DD_S – sinusoidal, DD_F – fluctuating, DD_{SF} – sinusoidal fluctuating; and ND, natural day). Dashed lines show linear fits through WT and mutant data points of one growth condition. Lower panels: the negative slopes of the fits correlate strongly with average photon flux density (PFD_{mean}; Table S10). (b) Φ_{PSII}–NPQ relationships at 20 or 60 s after transfer from HI to LI show a strong negative correlation. (a, b) Averages of $n = 3$–7 ± SE are shown. Some error bars are smaller than data point symbols and therefore not visible. Pearson correlation coefficient ρ and slope β are given for all data points of one measurement. For significant correlations, Pearson correlation coefficient ρ is given for all points (ρ_{all}) or those of phytotron-grown plants only ($\rho_{FD/DD}$; lower panel) with asterisks indicating *, $P < 0.05$; ***, $P < 0.0001$. Measurements were performed continuously between 2 and 10 h into the photoperiod by repeating a fixed sequence of different genotypes.

the HI phase (Fig. 2b). Multiple regression analyses revealed that most changes in the mutant NPQ phenotypes between conditions correlated with differences in PFD_{mean} or PFD_{var} (Fig. 2c; Table S8). PFD_{mean} had opposing effects on the mutant/WT NPQ ratios (i.e. the NPQ phenotypes) of *vccn1* and *kea3* during the HI phase: while the low NPQ phenotype of *vccn1* decreased and NPQ became more similar to WT, the high NPQ phenotype of *kea3* increased with PFD_{mean}. Strongly elevated HI-NPQ was seen in *kea3* grown under higher PFD_{mean}. The strongest effect of PFD_{mean} on the *vccn1* NPQ phenotype was found during the first measuring point at HI (30 s), while for the *kea3* NPQ phenotype, it was highest at 60 s HI. The second light factor, PFD_{var}, explained an increase in the high NPQ phenotype of *kea3* mutants during LI (Fig. 2c). The strongest effect was found at 60 s after transition from HI to LI. Multiple regression analyses also revealed a significant effect of PFD_{var} on the *vccn1* NPQ phenotype 5 min in the dark after the fluctuating light treatment (time point 6). To visualize the correlation with PFD_{mean} at HI and PFD_{var} at LI, NPQ ratios were plotted against the respective light factors and linear fits were performed (Fig. 2d,e).

Together, the results show that the functions of both VCCN1 and KEA3 respond oppositely to PFD_{mean} during a short HI phase in a sequential manner and reveal an enhancing effect of strong light fluctuations on the NPQ relaxation phenotype of *kea3* during LI.

Growth light intensity determines the impact of thylakoid ion transport on photosynthetic efficiency at high irradiances

To approximate light-environmental effects on photosynthetic capacity during the short light fluctuation, Φ_{PSII} was calculated. Across all genotypes from phytotron conditions, Φ_{PSII} correlated positively with PFD_{mean} during HI (Fig. S6a,b; Table S9). Gas exchange measurements were performed on WT, *kea3*, and *vccn1* from selected phytotron conditions, which confirmed the positive Φ_{PSII} correlation with PFD_{mean} during HI (Fig. S6c).

Nonphotochemical quenching correlated negatively with PFD_{mean} 60 s after the LI to HI transition (Fig. S6d; Table S9). The correlation was weaker for *kea3* than for the other two genotypes. This was expected because of the positive effect that PFD_{mean} had on KEA3-mediated NPQ suppression at this time point. Here also, the Φ_{PSII} correlation with PFD_{mean} was weaker for *kea3* than for the other two genotypes, which suggested Φ_{PSII} was affected as a result of changes in NPQ. Thus, we performed a systematic analysis of the NPQ and Φ_{PSII} relationships. After 30 s at HI, the overall inverse Φ_{PSII}-NPQ correlation was relatively weak (correlation coefficient $\rho = -0.50$; Fig. 3a, 30 s, upper panel). However, when Φ_{PSII}-NPQ relationships were determined separately for each of the light conditions, most were found to have much higher correlation coefficients (Table S10) and fitted negative slopes responded linearly to PFD_{mean} (Fig. 3a, 30 s, lower panel). After 1-min HI, overall correlation increased ($\rho_{all} = -0.73$; Fig. 3a, 60 s, upper panel), but the impact of PFD_{mean} on the fitted slopes remained strong (Fig. 3a, 60 s, lower panel). During NPQ relaxation in LI, Φ_{PSII} correlated near-linearly with NPQ, without evident environmental light effects on the relationships (Fig. 3b).

The data reveal that changes in NPQ, elicited by alterations of thylakoid ion transport, affect PSII quantum efficiency at HI with a linear dependency on PFD_{mean}. This may have been expected because of the overall increase in Φ_{PSII} with PFD_{mean}. The Φ_{PSII}–NPQ relationship during NPQ relaxation at LI, in turn, was much less affected by PFD_{mean}.

The induction of qE is shaped by light acclimation, thylakoid ion transport, and their interactions

Three environments with strongly differing effects on the NPQ phenotypes of *kea3* and *vccn1* (i.e. FD_L, FD_H, and DD_F) were selected to delineate light acclimation effects on VCCN1 and

Fig. 4 Time-resolved measurements reveal regulatory responses that follow a sudden jump in light intensity. (a) Both pmf components can be simultaneously observed by monitoring energy-dependent quenching (qE), which approximates changes in ΔpH, and the electrochromic shift (ECS), which reflects changes in membrane potential ($\Delta\psi$). S, stroma; L, lumen; TM, thylakoid membrane; pmf, proton motive force. (b) Spectroscopic setup with emitter (E), detector (D), and reference detector (R), which measures absorption in attached mature leaves near-simultaneously at six wavelengths (left) and spectra of leaf components that absorb at these wavelengths used for deconvolution of the qE and ECS signals (right). Component spectra were obtained as described in Table S2. The deconvolution approach was verified using *Arabidopsis thaliana* knockout mutants of the PsbS protein (*npq4*) and zeaxanthin epoxidase (*npq2*; Fig. S7). (c, d) Changes in the deconvoluted qE (qE_{535} (ΔA, rel); (c) and electrochromic shift signal (ECS (ΔA, rel); (d) of *A. thaliana* wild-type (WT) and two mutant alleles each of *kea3* and *vccn1* grown in FD_L (flat day low, left panel), FD_H (flat day high, middle panel), or DD_F (dynamic day fluctuating, right panel) during the transition from low irradiance (LI, 90 μmol photons m^{-2} s^{-1}) to high irradiance (HI, 900 μmol photons m^{-2} s^{-1}). Average traces of $n = 4$–$7 \pm$ SE are shown for the period of 15 s LI before and 60 s HI during the third light fluctuation, with one fluctuation comprising a sequence of 60 s HI, 20 s LI, 30 s darkness, and then 220 s LI. The amplitude of the initial ECS increase and the amplitude of the signal decay after the spike were used for calculating ECS relaxation capacity (Table 1). Absorbance measurements were performed between 2 and 10 h into the photoperiod by repeating a fixed sequence of different genotypes. (e, f) ECS_t as an estimate for total pmf (e) and adenosine triphosphate (ATP) synthase conductivity (g_{H^+}, (f)) determined from short dark pulses applied to the same fluctuating light setup as in c and d of WT, *kea3-1* and *vccn1-1* grown in FD_L (left), FD_H (middle), and DD_F (right). Averages are shown for $n = 4$–$6 \pm$ SE. Some error bars are smaller than data point symbols and therefore not visible. Red arrows indicate approximate time points of KEA3 activation as estimated from (d). Note that in (e and f), time resolution is small compared with c and d yielding no information on the actual g_{H^+} minimum, which may be before the second measuring point. Statistically significant differences to WT, determined by one-way ANOVA and the Tukey multiple comparison test, are indicated by asterisks with *, $P < 0.05$. Because of low signal-to-noise ratio at 520 nm in LI, ECS_t and g_{H^+} were averaged between the third and fourth fluctuations. (c–f) *y*-Axes were scaled to emphasize differences between genotypes. Signal amplitudes depend on pigment content and thus cannot be compared between conditions. (g) Model of the activity and function of VCCN1 and KEA3 during the HI phase as a function of time of plants from different growth light conditions. Red arrow sizes signify proton transport activity of ATP synthase, and blue and purple arrows indicate Cl^- and K^+ transport activities of VCCN1 and KEA3, respectively.

KEA3 activation and function at millisecond time resolution. We measured qE-related absorption changes at 535 nm (qE_{535}) as a proxy for the lumenal proton concentration, and the ECS *c.* 520 nm, which reports on the thylakoid membrane potential ($\Delta\psi$, Fig. 4a). For this, we performed near-simultaneous measurements at six different wavelengths between 475 and 545 nm

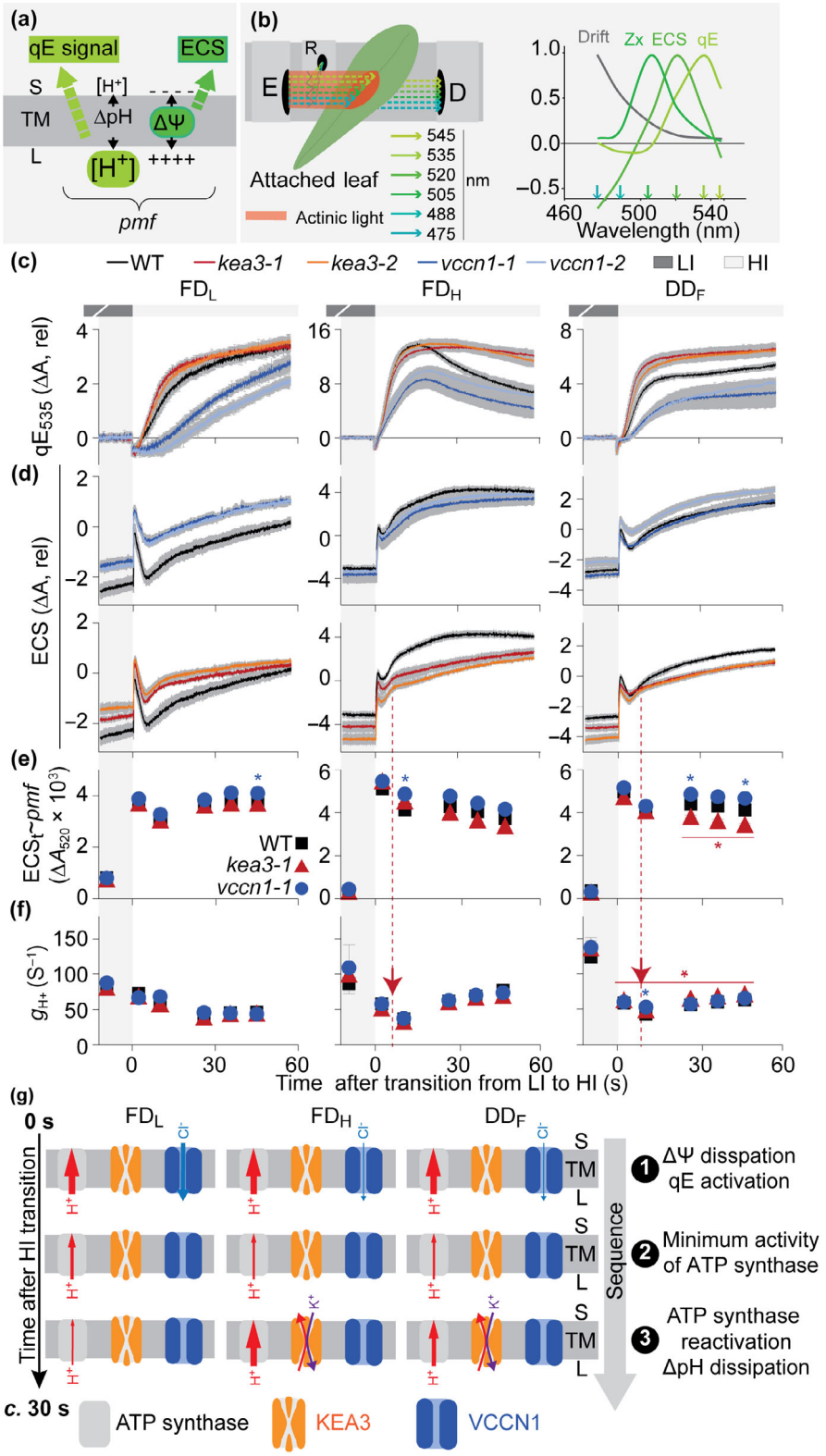

to obtain information on peaks and flanks of the two absorption spectra as well as to correct for other signals in this region (Fig. 4b). We validated this approach by analyzing mutants with differences in qE and Zx accumulation (Fig. S7). Additionally, we confirmed Chl*a* fluorescence-based NPQ results from WT and thylakoid ion transport mutants using the same spectrometer (Fig. S8a). No consistent differences in total chlorophyll and total carotenoid contents, visual leaf appearance, and rosette dry weight were observed between WT, *kea3*, and *vccn1* for a given light environment (Table S11; Figs S4a,b, S8b). This permitted the direct comparison of absorption signals between WT and mutants from the same condition. Also, no significant differences in KEA3 content were observed in WT and *vccn1* between the three conditions (Fig. S8c; Table S12).

In general, growth light conditions strongly affected the dynamic responses of both qE_{535} and ECS, to a sudden increase in light intensity (Fig. 4c,d; Tables S13, S14). Loss of VCCN1 or KEA3 further influenced these responses in an environment-dependent manner. Directly after the transition from LI to HI, loss of VCCN1 led to a lag in qE_{535} induction, which was more pronounced in FD_L than in DD_F and FD_H (Fig. 4c). A general feature of the ECS ($\Delta\psi$) response to the increase in light intensity was that it spiked within the first second after the shift, followed by varying degrees of ECS relaxation (Fig. 4d; Table 1). Both *kea3* and *vccn1* displayed a decreased capacity to relax the ECS signal when compared to WT from the same condition. The largest difference was found in FD_L between WT, which relaxed ECS back to LI levels, and *vccn1*, which only relaxed ECS to two-thirds of the initial incline.

During the entire HI phase, no qE_{535} differences were observed between *kea3* and WT from FD_L (Figs 4c, S8a). The *kea3* from FD_H and DD_F instead had higher qE_{535} signals than their corresponding WTs after initial similar induction kinetics (Fig. 4c). Thus, differences in qE_{535} recapitulated the observed changes in NPQ. The high qE_{535} in *kea3* from FD_H and DD_F was accompanied by lower ECS signals. While ECS showed a fast second rise in WT and *vccn1* at 6 and 8 s after the shift for FD_H and DD_F, respectively, the kinetics of this rise were much slower in *kea3*. A difference in this second ECS rise was particularly evident for *kea3* from FD_H, in which lower ECS as compared to WT preceded the higher qE_{535} signal by multiple seconds (Fig. 4c,d).

In summary, the results revealed *vccn1* to have decreased capacity for $\Delta\psi$ relaxation after the initial steep rise, coinciding with delayed qE_{535} induction. Both, $\Delta\psi$ relaxation capacity and qE induction, were most strongly impaired in *vccn1* from FD_L, then DD_F, and least in FD_H. This supports VCCN1 function during LI to HI transitions to be negatively affected by increasing growth light intensities. Interestingly, also *kea3* mutants showed a reduced capacity for $\Delta\psi$ relaxation, particularly in DD_F plants (Fig. 4d; Table 1). This may be explained by the dissipation of $\Delta\psi$ by outward K^+ flux requiring KEA3-mediated transport of K^+ into the lumen. However, compared with *vccn1*, the decreased capacity of *kea3* to relax $\Delta\psi$ after the initial spike had minor impact on qE_{535}. Instead, KEA3 contributed to decreases in qE_{535} at later time points after the LI to HI transition in plants from FD_H and DD_F. This was accompanied by KEA3-mediated increases in $\Delta\psi$ as measured by the ECS signal. These results can be explained by the following: a few seconds after the shift from LI to HI, KEA3 is activated in plants from FD_H and DD_F and lumenal protons are exchanged for stromal potassium; this decreases the proton concentration of the lumen and leads to simultaneous increases in the $\Delta\psi$ component of the pmf; as a result of the decrease in lumenal protons, qE is down-regulated.

To further determine whether ECS differences reflected changes at the level of pmf composition or total pmf, we determined the light–dark difference in the ECS signal at 520 nm as a proxy for light-induced pmf (ECS_t, Fig. 4e). For this, 0.5-s dark pulses were applied every 10 s throughout the measurement. Electrochromic shift decay kinetics were additionally used to derive the trans-thylakoid proton conductivity (g_{H^+}; Fig. 4f), as a measure for ATP synthase activity. The ECS_t (i.e. light-induced pmf) strongly increased after transition from LI to HI. As previously reported, *vccn1* had higher ECS_t as compared to WT (Herdean *et al.*, 2016). The timing after the shift from LI to HI depended on growth light condition: *vccn1* from FD_H and FD_L had higher ECS_t as compared to WT at 10 and 45 s in HI, respectively, and *vccn1* from DD_F at 26 and 46 s (Fig. 4e). The ECS_t was not influenced by lack of KEA3 under both FD conditions (Fig. 4e). The similar ECS_t values between WT and *kea3* from FD_H demonstrated that decreased ECS values in *kea3* from this condition reflected a lower $\Delta\psi$ and higher ΔpH contribution to the pmf. In DD_F, *kea3* plants showed reduced ECS_t along with the lower ECS signals at the later three measuring time points.

g_{H^+} decreased directly after the transition to HI and then increased again after 10 s in FD_H and DD_F, while continuing to decrease in FD_L until stabilizing after *c.* 30 s at a minimum level (Fig. 4f). Lack of both KEA3 and VCCN1 both positively affected g_{H^+} of DD_F-grown plants: *vccn1* had elevated g_{H^+} after

Table 1 Recovery of the electrochromic shift (ECS) signal after a LI to HI transition depends on both VCCN1 and KEA3.

Growth condition	ECS relaxation capacity (%)				
	WT	*kea3-1*	*kea3-2*	*vccn1-1*	*vccn1-2*
FD_L	95 ± 6^a	80 ± 5^b	81 ± 5^b	70 ± 2^c	67 ± 4^c
FD_H	26 ± 3^a	24 ± 6^{ab}	17 ± 3^b	23 ± 3^b	19 ± 1^b
DD_F	56 ± 5^a	31 ± 6^b	32 ± 2^b	37 ± 4^b	37 ± 2^b

The deconvoluted signal of the ECS *c.* 520 nm of *Arabidopsis thaliana* wild-type (WT) and two independent mutant alleles each for *kea3* and *vccn1* was recorded during the transition from low irradiation (LI, 90 μmol photons m^{-2} s^{-1}) to high irradiation (HI, 900 μmol photons m^{-2} s^{-1}) as shown in Fig. 4. Plants were selected from three different growth conditions ($FD_{L/H}$, flat day low/high; DD_F, dynamic day fluctuating). After the light transition, the ECS signal strongly increased and then decayed again. The ECS relaxation capacity was defined as the amplitude of the decayed signal relative to the amplitude of the initial increase. Averages of $n = 4–7 \pm$ SE are shown. Different lowercase letters in superscript indicate significant differences as determined by one-way ANOVA for genotypes of a given condition and the subsequent SNK multiple comparison.

10 s at HI and *kea3* throughout the entire HI period. Interestingly, KEA3 activation in HI, as deduced from increases in $\Delta\psi$ during the second phase of ECS incline within *c.* 10 s after transition to HI (present in WT, but lacking in *kea3*), coincided with increased g_{H^+} in all genotypes (Fig. 4d,f, red arrows). This finding suggests that the activities of ATP synthase and KEA3 are synchronized.

Together, the results shown in Fig. 4 and Table 1 propose the following sequential response to a 10-fold increase in light intensity (Fig. 4g): (1) the membrane potential, which initially spikes, is partially dissipated by passive ion flux across the thylakoid membrane to establish qE with a direct function of Cl^- via VCCN1; (2) proton conductivity of the ATP synthase reaches a minimum; and (3) adenosine triphosphate synthase is reactivated with the simultaneous dissipation of ΔpH by KEA3-mediated K^+/H^+ exchange, relaxing, or stabilizing qE. Responses (1) and (3) show strong growth light dependency.

The effect of KEA3 on qE relaxation after a HI to LI shift is not only due to direct activation

After transition back from HI to LI, qE_{535} behaved very similarly between the three conditions in both WT and *vccn1* and fully relaxed within 20 s (Fig. 5a). In all genotypes and all growth light conditions, ECS ($\Delta\psi$) collapsed immediately after the LI transition, followed by a recovery phase (Fig. 5b). The response of *kea3* to the HI to LI shift was markedly different from WT. qE_{535} of *kea3* from DD_F and FD_L showed little-to-no relaxation within the first 20 s after the shift. *kea3* from FD_H showed qE_{535} relaxation, but delayed as compared to WT. Electrochromic shift recovery after the initial drop was strikingly reduced in *kea3* from FD_L and DD_F and reached much lower levels as compared to WT at 20 s after the shift (Fig. 5b). In FD_H plants, the effect of the *kea3* lesion on $\Delta\psi$ after the HI to LI transition appeared to be minor. While ECS was much lower in *kea3* before the transition (see also Fig. 4d), it reached WT levels after *c.* 5 s in LI.

After the transition to LI, ECS_t (light-induced pmf) decreased, while g_{H^+} increased (Fig. 5c,d). No significant ECS_t differences were present between genotypes in LI, supporting that decreased ECS signals in *kea3* after the HI to LI shift represented a lower $\Delta\psi$ contribution to pmf in FD_L and DD_F. Interestingly, *vccn1* from FD_L and DD_F, the conditions under which we observed a stronger contribution of VCCN1 to $\Delta\psi$ dissipation at HI, showed an increase in g_{H^+} after 10 s in LI (Fig. 5d). These observations may be linked, but cannot be easily explained as additional differences in spectroscopic parameters are missing. The LI shift was followed by a dark phase to determine the contribution of $\Delta\psi$ and ΔpH to pmf 20 s after transition from HI to LI (Cruz *et al.*, 2001). Indeed, $\Delta\psi$ contribution to total pmf was significantly decreased in *kea3* as compared to the other genotypes from plants grown in FD_L and DD_F (Fig. 5e).

Together, our data support that KEA3 has an important function in the relaxation of qE after a HI to LI shift. In plants from FD_L and DD_F, KEA3 appears to directly lower the proton concentration of the lumen and thereby the ΔpH fraction of the pmf. In FD_H, lack of KEA3 resulted likewise in attenuated qE relaxation, however, without measurable differences in pmf composition. This finding suggests that in contrast to plants from the other two light environments, the applied light shift did not induce any KEA3 activity in FD_H-grown plants. By comparing qE_{535} dark relaxation of *kea3* from FD_L and DD_F, we found additional striking differences: in plants from FD_L, qE_{535} of *kea3* reached WT levels after a 30 s dark period, while in plants from DD_F, qE_{535} remained high as compared to WT and showed very slow relaxation kinetics in the dark. We thus reasoned that in comparison with WT, *kea3* mutants from FD_H and DD_F must contain (more of) at least one additional factor that slows down qE relaxation kinetics.

KEA3 suppresses Zx accumulation

We then investigated whether Zx could be the additional factor influencing qE relaxation kinetics. To this end, we measured pigment content 6 h into the light period. This analysis demonstrated that *kea3* mutants had strongly elevated Zx levels as compared to WT both in FD_H and DD_F, but not in FD_L (Fig. 6a). To investigate whether differences in Zx levels were light-dependent, we measured pigments of DD_F-grown plants after overnight dark treatment. Here, the Zx content was much lower as compared to 6 h in the light, and the difference between *kea3* and WT became smaller (Fig. 6a).

Together, our results propose an additional function for KEA3, which is to suppress Zx accumulation in growth regimes with high-light phases.

Excessive Zx delays the response of qE to KEA3-dependent pH changes in the lumen

To address the question of whether Zx levels interact with the proton transporting activity of KEA3 in shaping qE relaxation kinetics, we employed the *npq2* mutant, which lacks zeaxanthin epoxidase (ZEP) and thus has a strongly increased VAZ pool with 100% Zx (Figs 6b, S9a,b; Niyogi, 1998; Johnson *et al.*, 2009). We grew WT and *kea3* together with *npq2* and *npq2 kea3* double mutants (Armbruster *et al.*, 2014) in FD_L and DD_F and measured NPQ under light fluctuations (Fig. S9c,d; Table S15). In line with our findings from WT and *kea3*, a KEA3-dependent decrease in HI-NPQ in the *npq2* background was observed only in DD_F, but not in FD_L (Fig. S9c). This result suggested that KEA3-dependent differences in HI-NPQ between these two conditions were not strongly influenced by the high Zx levels present in *npq2*. Nonphotochemical quenching relaxation after the HI to LI transition was delayed in *npq2* as compared to WT, supporting that increased levels of Zx alone cause slower NPQ relaxation kinetics (Fig. 6c). Because of the short time frame of the LI period (4 min), we can assume relaxed NPQ to represent mainly qE. The *npq2 kea3-1* mutant exhibited slower NPQ relaxation kinetics as compared to *kea3-1*, demonstrating that high Zx levels and loss of KEA3 have an additive effect on slowing down NPQ (qE) relaxation. The further delay of NPQ relaxation by high Zx levels in *npq2 kea3-1* as compared to *kea3*

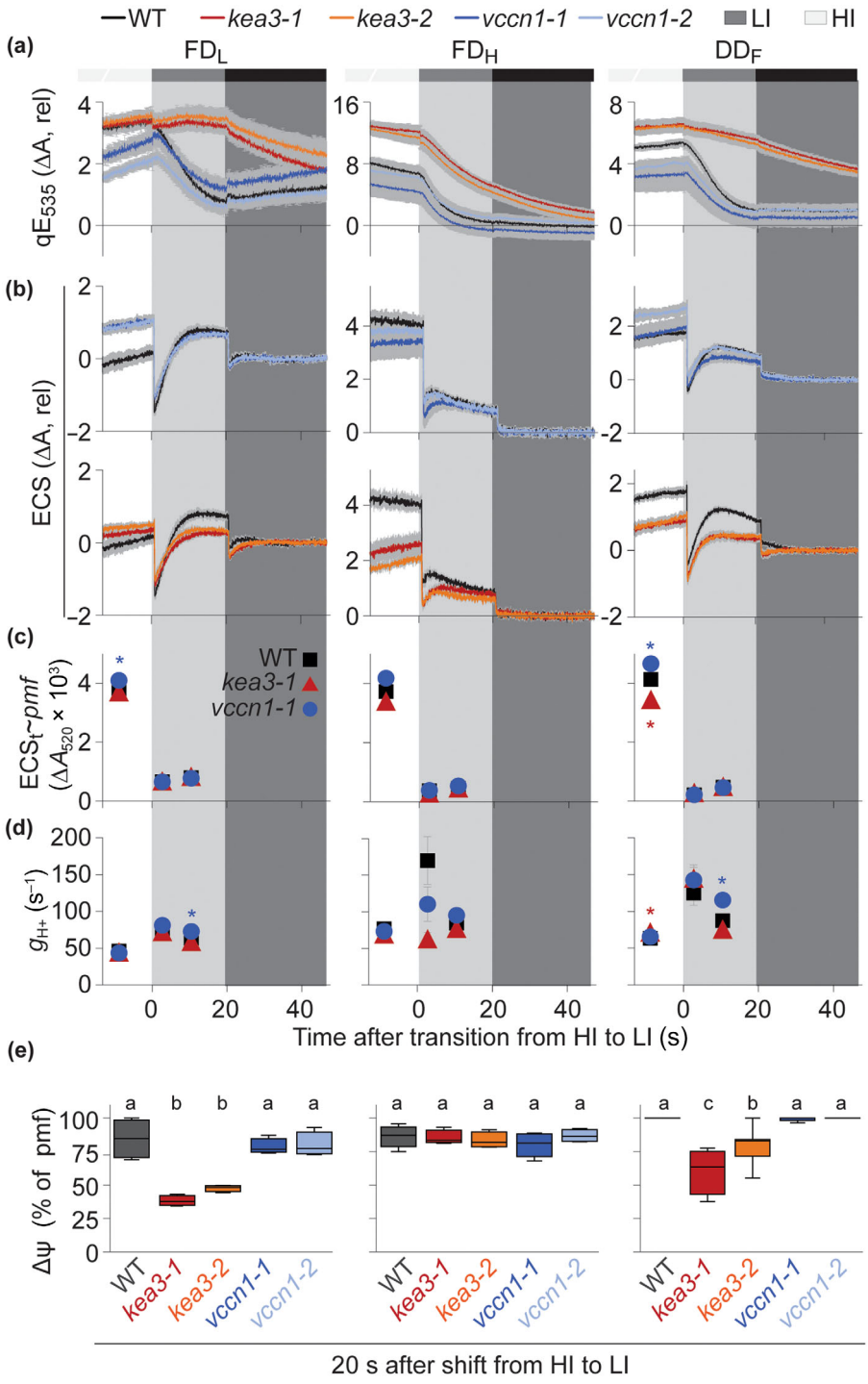

Fig. 5 KEA3 function in qE relaxation is not restricted to direct changes in proton motive force (pmf) composition. (a, b) Changes in the deconvoluted qE (qE_{535} (ΔA, rel); (a) and electrochromic shift signals (ECS (ΔA, rel); (b) of *Arabidopsis thaliana* wild-type (WT) and two mutant alleles each of *kea3* and *vccn1* grown in FD_L (flat day low, left panel), FD_H (flat day high, middle panel), or DD_F (dynamic day fluctuating, right panel) during the transition from high irradiance (HI, 900 μmol photons m^{-2} s^{-1}) to low irradiance (LI, 90 μmol photons m^{-2} s^{-1}). Average traces of $n = 4–7 \pm$ SE are shown for the period of 15-s HI, 20-s LI, and 30-s darkness during the third light fluctuation after the start of the measurement, with one fluctuation comprising a sequence of 60 s HI, 20 s LI, 30 s darkness, and then 220 s LI. (c, d) ECS_t as an estimate for total pmf (c) and adenosine triphosphate synthase conductivity (g_{H^+}, d) determined from short dark pulses applied to the same fluctuating light setup as in (a and b). Averages are shown for $n = 4–6 \pm$ SE. Some error bars were smaller than data point symbols and therefore not visible. Statistically significant differences to WT, determined by one-way ANOVA and the Tukey multiple comparison test, are indicated by asterisks with *, $P < 0.05$. Because of low signal-to-noise ratio at 520 nm in LI, ECS_t and g_{H^+} were averaged between the third and fourth fluctuations. (e) The $\Delta\psi$ component of the pmf was determined 20 s after the HI to LI shift. Averages of $n = 4–7$ are provided. The lower and upper boundaries of the box represent the 25th and 75th percentile, and the median is indicated by the middle line. Whiskers extend to the maximum and minimum. Lowercase letters above the box plots indicate significant differences between genotypes as determined by the two-way ANOVA and subsequent SNK multiple comparison test. (a–d) *y*-Axes were scaled to emphasize differences between genotypes. Signal amplitudes depend on pigment content and thus cannot be compared between conditions.

was less pronounced under DD_F than under FD_L. This finding is in line with *kea3-1* having increased Zx in DD_F, which delays qE relaxation. Comparing NPQ relaxation kinetics between the different genotypes showed that *kea3* is strongly delayed at the first measuring points 20 s after the transition (Fig. 6c). Particularly in DD_F, there was only little difference between *kea3-1* and *npq2 kea3-1* at this time point, suggesting minor influence of *npq2*-dependent higher Zx on NPQ within the first 20 s. At subsequent time points, however, the double mutant had strongly enhanced NPQ as compared to *kea3*. This observation hints at proton export from the lumen by KEA3 preceding some of the effects of Zx on NPQ relaxation.

Discussion

This study has addressed the question of how light-environmental acclimation interacts with the function of thylakoid ion transport during light fluctuations. From different growth environments, we extracted two light factors, light intensity (PFD_{mean}) and variability (PFD_{var}). Our data established that

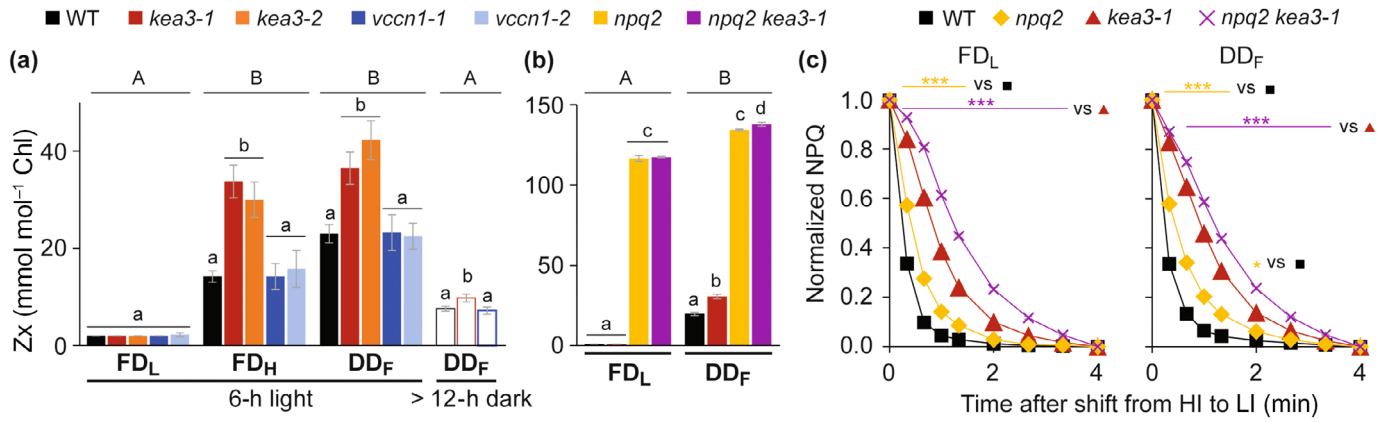

Fig. 6 KEA3 suppresses zeaxanthin (Zx) in the light, with high Zx accumulation delaying the response of nonphotochemical quenching (NPQ) to changes in lumen pH. (a) Zeaxanthin content was determined for *Arabidopsis thaliana* wild-type (WT) and two mutant alleles each of *kea3* and *vccn1* as mmol mol^{-1} Chl. Samples were taken 6 h into the light period for FD_L (flat day low), FD_H (flat day high), or DD_F (dynamic day fluctuating) and after an overnight dark phase for DD_F (> 12-h dark). In the light period, DD_F plants were sampled only during the low-light phase of the fluctuations. (b) Zeaxanthin content of WT, *kea3-1*, *npq2*, and *npq2 kea3-1* from FD_L or DD_F 6 h into the light period. (a, b) Note that differences between pigment content from thylakoids (Table S3) and whole rosette pigments can be explained by differences in sampling procedure. Averages of $n = 4$–$5 \pm$ SE are shown. Capital letters indicate significantly different groups between treatments, and lowercase letters between genotypes within one treatment by the two-way ANOVA and the Tukey (a) or SNK (b) multiple comparison test. (c) Normalized NPQ relaxation of WT, *kea3-1*, *npq2*, and *npq2 kea3* grown in FD_L (left panel) or DD_F (right panel) after a shift from high irradiance (HI, 900 μmol photons m^{-2} s^{-1}) to low irradiance (LI, 90 μmol photons m^{-2} s^{-1}) during the third fluctuation of a fluctuating light treatment with one fluctuation comprising of a sequence of 1 min HI and 4 min LI. Averages of $n = 6 \pm$ SE are shown. Measurements were performed continuously between 2 and 10 h into the photoperiod by repeating a fixed sequence of different genotypes. Statistically significant differences between *nqp2 kea3* and *kea3* or *npq2* and WT, as determined by one-way ANOVA and the Tukey multiple comparison test, are indicated by asterisks in yellow or purple, respectively, with *, $P < 0.05$ and ***, $P < 0.05$. Some error bars were smaller than data point symbols and therefore not visible. Values for NPQ in PSII quantum efficiency (Φ_{PSII}) during the entire fluctuating light treatment and corresponding statistical analyses can be found in Fig. S9(c,d) and Table S15, respectively.

photosynthetic capacity strongly correlates with PFD_{mean} and revealed that levels of de-epoxidized xanthophylls (Zx) rise with PFD_{var} (Fig. 7a). We confirmed the previously published function of KEA3 in plants from low growth light conditions, which is to accelerate NPQ/qE relaxation in LI (Armbruster *et al.*, 2014). In this study, we found KEA3-mediated NPQ/qE suppression during high-light phases, in which it correlated positively with PFD_{mean}; and, respond to PFD_{var} during relaxation. Additionally, we revealed a function for KEA3 in the suppression of Zx accumulation. The NPQ phenotype of *vccn1* in HI, published earlier for low growth light conditions (Duan *et al.*, 2016; Herdean *et al.*, 2016), was shown to disappear with increasing PFD_{mean}. We propose that at least some of the effects of PFD_{mean} on the activities of both KEA3 and VCCN1 during short high-light phases can be explained by changes in photosynthetic capacity. Additionally, we link the PFD_{var} dependence of the *kea3* NPQ/qE relaxation phenotype to an interaction of Zx levels with KEA3 activity.

The results of our spectroscopic analyses of photosynthesis during a 10-fold change in light intensity (used as an approximation for strong variations found in nature; Fig. 7b) are summarized in two models.

Jump in light intensity: VCCN1 activity anticipates metabolic limitations, which in turn precede KEA3 activation

During steady-state photosynthesis, light reactions and downstream metabolism are balanced (Fig. 7c). A sudden jump in light intensity leads to rates of light reactions initially exceeding those of downstream metabolism. This is due to a lag in the activation of the carbon-fixing Calvin–Benson–Bassham cycle, which is tied to a number of changes that occur on the second-to-minute time scale. These involve stromal pH and magnesium, redox regulation, and intermediate metabolite pools (Werdan *et al.*, 1975; Portis & Heldt, 1976; Schürmann *et al.*, 1976; Purczeld *et al.*, 1978; Stitt *et al.*, 2010). Increased rates of electron and proton transport cause the thylakoid membrane potential to rise. $\Delta\psi$ dissipation by ion flux involving the VCCN1 Cl^- channel facilitates an increase in the lumen proton concentration and activation of qE. Our data suggest that the extent of $\Delta\psi$ dissipation after a jump in light intensity negatively correlates with growth light intensity. Acclimation to low growth light favors strong $\Delta\psi$ dissipation after an increase in light intensity, which is necessary for fast qE induction. Following $\Delta\psi$ dissipation, the activity of the ATP synthase (estimated by g_{H^+}) reaches a minimum. This can be explained by high ATP : ADP ratios and low availability of inorganic phosphate, which result from the lag in CBB-cycle activation (Fig. 7c; Takizawa *et al.*, 2008; Morales *et al.*, 2017). As soon as the CBB cycle catches up with the light reactions, rates of ATP synthase rise again. Additionally, KEA3 is activated to rapidly dissipate ΔpH, deactivate qE, and upregulate PSII activity. The qE deactivation may additionally be accelerated by KEA3-mediated Zx-suppression (next paragraph). This last phase in high light, which is characterized by the near-simultaneous activation of KEA3 and ATP synthase and qE relaxation, is missing in plants grown under low light intensities (i.e. FD_L). Together, these findings are in line with KEA3 being controlled

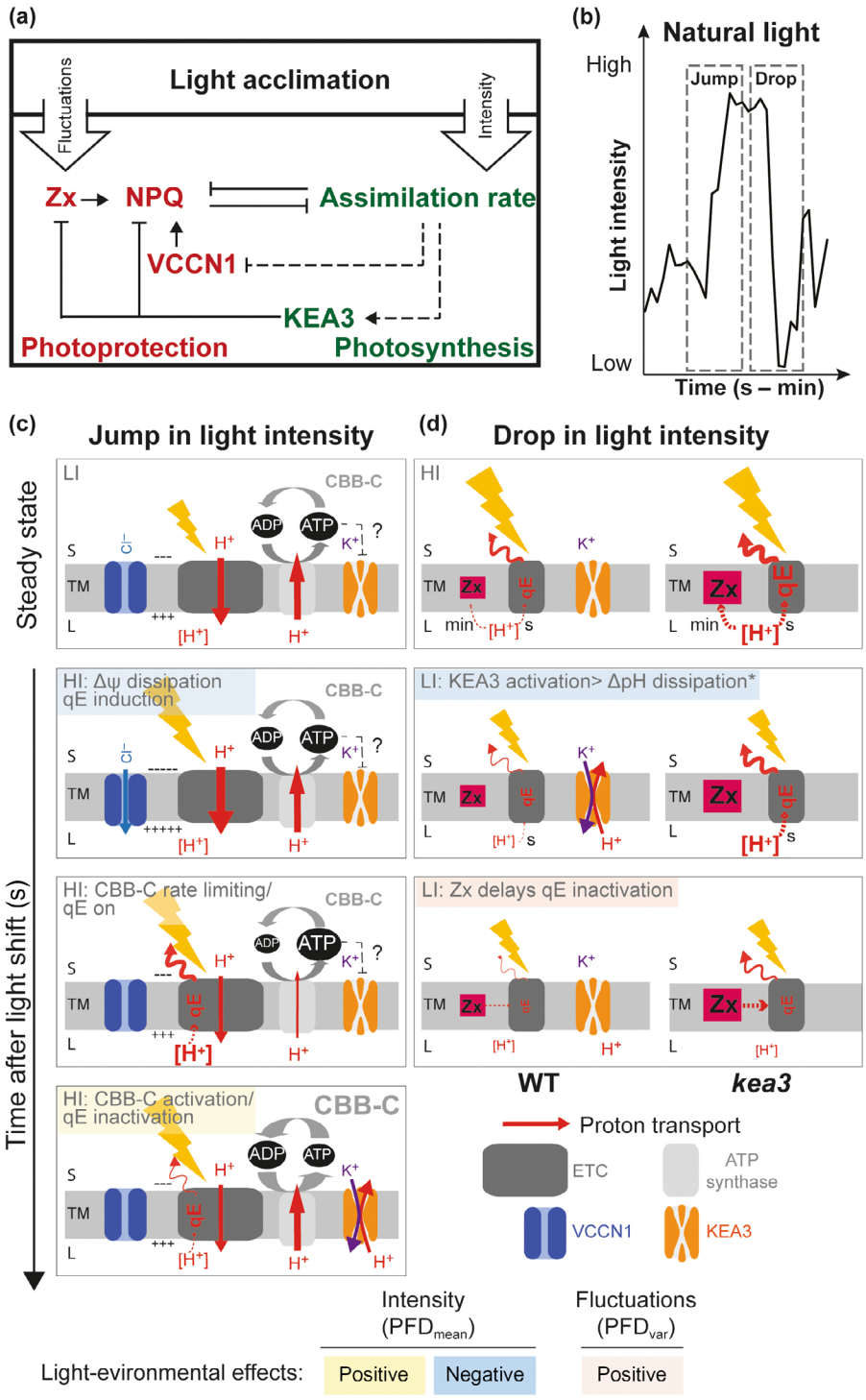

by rates of downstream metabolism and activation occurring in response to high CBB-cycle activity. The regulatory C-terminus of KEA3 contains a nucleotide-binding domain, which may render KEA3 activity responsive to ATP/ADP or NADPH/NADP$^+$ (Armbruster *et al.*, 2016; Wang *et al.*, 2017; Li *et al.*, 2021; Uflewski *et al.*, 2021).

The loss of KEA3 but not VCCN1 affects Zx accumulation in plants grown at higher light intensities. Zeaxanthin accumulates when VDE activity in total exceeds that of ZEP, which converts Zx back to Vx. The WT-like accumulation of Zx in *vccn1*, despite measurable differences in qE under high light, must thus derive from a similar ratio of VDE/ZEP activities as in WT. One explanation is that the activities of both xanthophyll-cycle enzymes are WT-like in *vccn1*. This would assume VDE to have a lower pH activation threshold than PsbS, the activation of which is the main contributor to qE. An alternative explanation

Fig. 7 Model of environmental effects on dynamic photosynthesis and interactions with thylakoid ion transport. (a) In dynamic light environments, the switch between photoprotection and photosynthesis is governed by light acclimation, which interacts with the functions of VCCN1 and KEA3. Light fluctuations (i.e. PFD_{var}) are the main environmental factors boosting zeaxanthin (Zx) accumulation, while daily light intensity (i.e. PFD_{mean}) is the main environmental factor driving assimilation capacity. VCCN1 accelerates the photoprotective response by increasing nonphotochemical quenching (NPQ), while KEA3 supports photosynthesis by downregulating NPQ and levels of Zx. In short phases of high light intensity, the activation of both ion transport proteins is correlated with growth light intensity, suggesting assimilation rate to affect VCCN1 negatively and KEA3 positively. (b) Scheme of light intensity variations found in nature. (c) Time-resolved model illustrating the response of the photosynthetic proton circuit to a sudden jump in light intensity (from low irradiance (LI) to high irradiance (HI)): proton translocation into the lumen increases with light intensity. VCCN1 facilitates Cl^- flux and thereby contributes to the dissipation of the membrane potential ($\Delta\psi$) and concurrent increase in the lumen proton concentration [H^+]. The energy-dependent component of NPQ (qE) is activated, while adenosine triphosphate (ATP) synthase conductivity reaches a minimum. The ATP synthase reactivation coincides with the activation of KEA3, which lowers the proton concentration of the lumen and thereby decreases qE. Phases involving thylakoid ion transporter activity are shaped by daily growth light intensity. Because KEA3 activation coincides with a rise in the activity of ATP synthase, we propose KEA3 may be negatively regulated by the ATP : ADP ratio. (d) Time-resolved model illustrating the two functions of KEA3 in shaping qE relaxation kinetics during a sudden drop in light intensity (from HI to LI): by suppressing Zx accumulation at HI and rapidly downregulating the lumenal proton concentration directly after the decrease in light intensity. Note that while all other light-environment effects are derived from multiple regression analyses results of eight different conditions, the negative effect of PFD_{mean} on KEA3 activation in LI is based on an estimation using the proton motive force partitioning results of three selected light environments only (this exception is denoted by an asterisk). (c, d) CBB-C, CBB cycle; ETC, electron transport chain; S, stroma; L, lumen; TM, thylakoid membrane. The size of the lightning bold signifies light intensity. Red dashed arrows indicate positive regulatory effects of the proton concentration of the lumen. Arrow sizes indicate flux and font sizes concentrations (ATP, ADP, H^+) or activity (CBB cycle).

would be that VDE activity is higher in *vccn1* than in WT, but is matched by increased ZEP activity. The ZEP activity has been shown to respond to multiple factors including the redox state of the chloroplast stroma (Siefermann & Yamamoto, 1975; Bethmann *et al.*, 2019).

Drop in light intensity: KEA3 drives the inactivation of energy dissipation in a bifactorial manner

We show in this study that the role of KEA3 in NPQ/qE relaxation after a drop in light intensity is not restricted to its direct proton export activity (Fig. 7d). Our data suggest that Zx-suppression by KEA3 in plants grown under elevated PFD_{mean} contributes to their NPQ/qE relaxation kinetics. The KEA3 activity likely reduces the accumulation of Zx indirectly by pH-dependent inactivation of VDE. The *kea3* NPQ/qE relaxation phenotype correlated positively with PFD_{var}. This finding is in line with *kea3* from such a condition (i.e. DD_F) exhibiting both, high levels of Zx, and HI to LI transition-induced activation of KEA3 activity. By analyzing KEA3 function in the *npq2* mutants with high levels of Zx, we confirmed that KEA3-mediated proton export from the lumen affects qE relaxation as a function of Zx levels after a drop in light intensity. Together, our data suggest that high Zx delays the downregulation of qE triggered by KEA3-mediated decreases in the lumen proton concentration. Thus, it supports a model, in which Zx plays a major role in qE deactivation kinetics (Niyogi, 1998; Nilkens *et al.*, 2010).

Conclusion

Our results demonstrate that growth light acclimation strongly impacts the functions of both thylakoid ion transport proteins, KEA3 and VCCN1, in the rapid response of photosynthesis to short light fluctuations. This discovery mandates potential strategies to enhance plant productivity by modulating thylakoid ion transport to consider the effects of the reported light factors. A complex picture emerges for KEA3-mediated NPQ relaxation, which responds to both light intensity and variability.

Acknowledgements

We recognize P. Pieloch for excellent technical support and thank M.A. Schöttler for valuable discussions and help with the phytotrons and with the gas exchange measurements. We acknowledge help with plant cultivation provided by the Max Planck Institute-MP GreenTeam. UA and DMK are supported by the 3rd call ERA-CAPS grant (NSF IOS-1847193 and DFG AR 808/4-1). UA received funding from the DFG (AR 808/5-1) and the Max Planck Society. We would like to thank anonymous reviewers for their valuable comments. Open Access funding enabled and organized by Projekt DEAL.

Author contributions

UA and TB designed the study. TB performed most of the experimental work with help from JR and KS and supervision from VCG during the early stage of the study. K Korkmaz prepared thylakoids, which were analyzed by JE and IF. PJ performed pigment analyses. EK set up the phytotron for random light fluctuations. K Köhl helped with the polytunnel experiments and performed statistical analyses. JAC and DMK designed and supervised the absorption spectroscopy approach, which was interpreted by UA, TB and DMK. DMK validated the approach by using appropriate mutants. DDS helped analyzing spectroscopy data. UA and TB wrote the manuscript with contributions and input from all authors.

ORCID

Ute Armbruster https://orcid.org/0000-0002-8814-8207
Thekla Bismarck von https://orcid.org/0000-0002-8523-5313
Viviana Correa Galvis https://orcid.org/0000-0002-8092-9148
Jeffrey A. Cruz https://orcid.org/0000-0003-1098-5176
Jürgen Eirich https://orcid.org/0000-0003-0963-1872
Iris Finkemeier https://orcid.org/0000-0002-8972-4026

Peter Jahns https://orcid.org/0000-0002-5340-1153
Karin Köhl https://orcid.org/0000-0003-3912-9912
Elias Kaiser https://orcid.org/0000-0002-9081-9604
David M. Kramer https://orcid.org/0000-0003-2181-6888
Deserah D. Strand https://orcid.org/0000-0002-6179-7901

Data availability

Raw proteomics data were deposited via JPOST (Moriya *et al.*, 2019) under the identifier JPST001271 (https://repository.jpostdb.org). Additionally, the script to generate sinusoidal day with random light fluctuations (DD_{SF}) in the phytotron is available online (https://github.com/EliasKaiser/Fluctuations/blob/main/190614_Lightfleck_program.R).

References

Alter P, Dreissen A, Luo F-L, Matsubara S. 2012. Acclimatory responses of Arabidopsis to fluctuating light environment: comparison of different sunfleck regimes and accessions. *Photosynthesis Research* **113**: 221–237.

Armbruster U, Carrillo LR, Venema K, Pavlovic L, Schmidtmann E, Kornfeld A, Jahns P, Berry JA, Kramer DM, Jonikas MC. 2014. Ion antiport accelerates photosynthetic acclimation in fluctuating light environments. *Nature Communications* **5**: 5439.

Armbruster U, Leonelli L, Correa Galvis V, Strand D, Quinn EH, Jonikas MC, Niyogi KK. 2016. Regulation and levels of the thylakoid K^+/H^+ antiporter KEA3 shape the dynamic response of photosynthesis in fluctuating light. *Plant & Cell Physiology* **57**: 1557–1567.

Arnoux P, Morosinotto T, Saga G, Bassi R, Pignol D. 2009. A structural basis for the pH-dependent xanthophyll cycle in *Arabidopsis thaliana*. *Plant Cell* **21**: 2036–2044.

Athanasiou K, Dyson BC, Webster RE, Johnson GN. 2009. Dynamic acclimation of photosynthesis increases plant fitness in changing environments. *Plant Physiology* **152**: 366–373.

Bailey S, Horton P, Walters RG. 2004. Acclimation of *Arabidopsis thaliana* to the light environment: the relationship between photosynthetic function and chloroplast composition. *Planta* **218**: 793–802.

Bailey S, Walters RG, Jansson S, Horton P. 2001. Acclimation of *Arabidopsis thaliana* to the light environment: the existence of separate low light and high light responses. *Planta* **213**: 794–801.

Baker NR. 2008. Chlorophyll fluorescence: a probe of photosynthesis *in vivo*. *Annual Review of Plant Biology* **59**: 89–113.

Bethmann S, Melzer M, Schwarz N, Jahns P. 2019. The zeaxanthin epoxidase is degraded along with the D1 protein during photoinhibition of photosystem II. *Plant Direct* **3**: e00185.

Bilger W, Björkman O, Thayer SS. 1989. Light-induced spectral absorbance changes in relation to photosynthesis and the epoxidation state of xanthophyll cycle components in cotton leaves. *Plant Physiology* **91**: 542–551.

Briantais JM, Vernotte C, Picaud M, Krause GH. 1979. A quantitative study of the slow decline of chlorophyll a fluorescence in isolated chloroplasts. *Biochimica et Biophysica Acta* **548**: 128–138.

Cox J, Mann M. 2008. MaxQuant enables high peptide identification rates, individualized p.p.b.-range mass accuracies and proteome-wide protein quantification. *Nature Biotechnology* **26**: 1367–1372.

Cruz JA, Sacksteder CA, Kanazawa A, Kramer DM. 2001. Contribution of electric field ($\Delta\psi$) to steady-state transthylakoid proton motive force (*pmf*) *in vitro* and *in vivo*. Control of *pmf* parsing into $\Delta\psi$ and ΔpH by ionic strength. *Biochemistry* **40**: 1226–1237.

Demmig B, Winter K, Krüger A, Czygan F-C. 1987. Photoinhibition and zeaxanthin formation in intact leaves: a possible role of the xanthophyll cycle in the dissipation of excess light energy. *Plant Physiology* **84**: 218–224.

Demmig-Adams B, Adams WW III, Barker DH, Logan BA, Bowling DR, Verhoeven AS. 1996. Using chlorophyll fluorescence to assess the fraction of absorbed light allocated to thermal dissipation of excess excitation. *Physiologia Plantarum* **98**: 253–264.

Duan Z, Kong F, Zhang L, Li W, Zhang J, Peng L. 2016. A bestrophin-like protein modulates the proton motive force across the thylakoid membrane in Arabidopsis. *Journal of Integrative Plant Biology* **58**: 848–858.

Dukic E, Herdean A, Cheregi O, Sharma A, Nziengui H, Dmitruk D, Solymosi K, Pribil M, Spetea C. 2019. K^+ and Cl^- channels/transporters independently fine-tune photosynthesis in plants. *Scientific Reports* **9**: 8639.

Färber A, Young AJ, Ruban AV, Horton P, Jahns P. 1997. Dynamics of xanthophyll-cycle activity in different antenna subcomplexes in the photosynthetic membranes of higher plants (the relationship between zeaxanthin conversion and nonphotochemical fluorescence quenching). *Plant Physiology* **115**: 1609–1618.

Flannery SE, Hepworth C, Wood WHJ, Pastorelli F, Hunter CN, Dickman MJ, Jackson PJ, Johnson MP. 2021. Developmental acclimation of the thylakoid proteome to light intensity in Arabidopsis. *The Plant Journal* **105**: 223–244.

Golding AJ, Joliot P, Johnson GN. 2005. Equilibration between cytochrome f and P700 in intact leaves. *Biochimica et Biophysica Acta (BBA) – Bioenergetics* **1706**: 105–109.

Hager A. 1969. Lichtbedingte pH-Erniedrigung in einem Chloroplasten-Kompartiment als Ursache der enzymatischen Violaxanthin- → Zeaxanthin-Umwandlung; Beziehungen zur Photophosphorylierung. *Planta* **89**: 224–243.

Hall CC, Cruz J, Wood M, Zegarac R, DeMars D, Carpenter J, Kanazawa A, Kramer D. 2013. Photosynthetic measurements with the idea spec: an integrated diode emitter array spectrophotometer/fluorometer. In: Kuang T, Lu C, Zhang L, eds. *Photosynthesis research for food, fuel and the future*. Advanced Topics in Science and Technology in China. Berlin, Heidelberg & Germany: Springer, 184–188.

Hartel H, Lokstein H, Grimm B, Rank B. 1996. Kinetic studies on the xanthophyll cycle in barley leaves (influence of antenna size and relations to nonphotochemical chlorophyll fluorescence quenching). *Plant Physiology* **110**: 471–482.

Herdean A, Teardo E, Nilsson AK, Pfeil BE, Johansson ON, Unnep R, Nagy G, Zsiros O, Dana S, Solymosi K *et al.* 2016. A voltage-dependent chloride channel fine-tunes photosynthesis in plants. *Nature Communications* **7**: 11654.

Holt NE, Zigmantas D, Valkunas L, Li XP, Niyogi KK, Fleming GR. 2005. Carotenoid cation formation and the regulation of photosynthetic light harvesting. *Science* **307**: 433–436.

Johnson MP, Goral TK, Duffy CD, Brain AP, Mullineaux CW, Ruban AV. 2011. Photoprotective energy dissipation involves the reorganization of photosystem II light-harvesting complexes in the grana membranes of spinach chloroplasts. *Plant Cell* **23**: 1468–1479.

Johnson MP, Pérez-Bueno ML, Zia A, Horton P, Ruban AV. 2009. The zeaxanthin-independent and zeaxanthin-dependent qE components of nonphotochemical quenching involve common conformational changes within the photosystem II antenna in Arabidopsis. *Plant Physiology* **149**: 1061–1075.

Kaiser E, Correa Galvis V, Armbruster U. 2019. Efficient photosynthesis in dynamic light environments: a chloroplast's perspective. *Biochemical Journal* **476**: 2725–2741.

Kaiser E, Morales A, Harbinson J. 2017. Fluctuating light takes crop photosynthesis on a rollercoaster ride. *Plant Physiology* **176**: 977–989.

Kanazawa A, Kramer DM. 2002. *In vivo* modulation of nonphotochemical exciton quenching (NPQ) by regulation of the chloroplast ATP synthase. *Proceedings of the National Academy of Sciences, USA* **99**: 12789–12794.

Kulak NA, Pichler G, Paron I, Nagaraj N, Mann M. 2014. Minimal, encapsulated proteomic-sample processing applied to copy-number estimation in eukaryotic cells. *Nature Methods* **11**: 319–324.

Külheim C, Ågren J, Jansson S. 2002. Rapid regulation of light harvesting and plant fitness in the field. *Science* **297**: 91–93.

Kunz HH, Gierth M, Herdean A, Satoh-Cruz M, Kramer DM, Spetea C, Schroeder JI. 2014. Plastidial transporters KEA1, -2, and -3 are essential for chloroplast osmoregulation, integrity, and pH regulation in Arabidopsis. *Proceedings of the National Academy of Sciences, USA* **111**: 7480–7485.

Lassowskat I, Hartl M, Hosp F, Boersema PJ, Mann M, Finkemeier I. 2017. Dimethyl-labeling-based quantification of the lysine acetylome and proteome of plants. *Methods in Molecular Biology* **1653**: 65–81.

Li M, Svoboda V, Davis G, Kramer D, Kunz HH, Kirchhoff H. 2021. Impact of ion fluxes across thylakoid membranes on photosynthetic electron transport and photoprotection. *Nature Plants* **7**: 979–988.

Li X-P, Björkman O, Shih C, Grossman AR, Rosenquist M, Jansson S, Niyogi KK. 2000. A pigment-binding protein essential for regulation of photosynthetic light harvesting. *Nature* **403**: 391–395.

Li X-P, Gilmore AM, Caffarri S, Bassi R, Golan T, Kramer D, Niyogi KK. 2004. Regulation of photosynthetic light harvesting involves intrathylakoid lumen pH sensing by the PsbS protein. *Journal of Biological Chemistry* **279**: 22866–22874.

Long SP, Taylor SH, Burgess SJ, Carmo-Silva E, Lawson T, Souza APD, Leonelli L, Wang Y. 2022. Into the shadows and back into sunlight: photosynthesis in fluctuating light. *Annual Review of Plant Biology* **73**: 617–648.

Matthews JSA, Vialet-Chabrand S, Lawson T. 2018. Acclimation to fluctuating light impacts the rapidity of response and diurnal rhythm of stomatal conductance. *Plant Physiology* **176**: 1939–1951.

Mishra Y, Jänkänpää HJ, Kiss AZ, Funk C, Schröder WP, Jansson S. 2012. Arabidopsis plants grown in the field and climate chambers significantly differ in leaf morphology and photosystem components. *BMC Plant Biology* **12**: 6.

Mitchell P. 1966. Chemiosmotic coupling in oxidative and photosynthetic phosphorylation. *Biological Reviews of the Cambridge Philosophical Society* **41**: 445–502.

Morales A, Yin X, Harbinson J, Driever SM, Molenaar J, Kramer DM, Struik PC. 2017. *In silico* analysis of the regulation of the photosynthetic electron transport chain in C_3 plants. *Plant Physiology* **176**: 1247–1261.

Morgan MJ, Lehmann M, Schwarzländer M, Baxter CJ, Sienkiewicz-Porzucek A, Williams TC, Schauer N, Fernie AR, Fricker MD, Ratcliffe RG *et al.* 2008. Decrease in manganese superoxide dismutase leads to reduced root growth and affects tricarboxylic acid cycle flux and mitochondrial redox homeostasis. *Plant Physiology* **147**: 101–114.

Moriya Y, Kawano S, Okuda S, Watanabe Y, Matsumoto M, Takami T, Kobayashi D, Yamanouchi Y, Araki N, Yoshizawa AC *et al.* 2019. The jPOST environment: an integrated proteomics data repository and database. *Nucleic Acids Research* **47**: D1218–D1224.

Nilkens M, Kress E, Lambrev P, Miloslavina Y, Müller M, Holzwarth AR, Jahns P. 2010. Identification of a slowly inducible zeaxanthin-dependent component of non-photochemical quenching of chlorophyll fluorescence generated under steady-state conditions in Arabidopsis. *Biochimica et Biophysica Acta (BBA) – Bioenergetics* **1797**: 466–475.

Niyogi KK. 1998. Arabidopsis mutants define a central role for the xanthophyll cycle in the regulation of photosynthetic energy conversion. *Plant Cell* **10**: 1121–1134.

Pescheck F, Bilger W. 2019. High impact of seasonal temperature changes on acclimation of photoprotection and radiation-induced damage in field grown *Arabidopsis thaliana*. *Plant Physiology and Biochemistry* **134**: 129–136.

Portis AR, Heldt HW. 1976. Light-dependent changes of the Mg^{2+} concentration in the stroma in relation to the Mg^{2+} dependency of CO_2 fixation in intact chloroplasts. *Biochimica et Biophysica Acta (BBA) – Bioenergetics* **449**: 434–446.

Purczeld P, Chon CJ, Portis AR Jr, Heldt HW, Heber U. 1978. The mechanism of the control of carbon fixation by the pH in the chloroplast stroma. Studies with nitrite-mediated proton transfer across the envelope. *Biochimica et Biophysica Acta* **501**: 488–498.

Sacharz J, Giovagnetti V, Ungerer P, Mastroianni G, Ruban AV. 2017. The xanthophyll cycle affects reversible interactions between PsbS and light-harvesting complex II to control non-photochemical quenching. *Nature Plants* **3**: 16225.

Sacksteder CA, Jacoby ME, Kramer DM. 2001. A portable, non-focusing optics spectrophotometer (NoFOSpec) for measurements of steady-state absorbance changes in intact plants. *Photosynthesis Research* **70**: 231–240.

Sacksteder CA, Kanazawa A, Jacoby ME, Kramer DM. 2000. The proton to electron stoichiometry of steady-state photosynthesis in living plants: a proton-pumping Q cycle is continuously engaged. *Proceedings of the National Academy of Sciences, USA* **97**: 14283–14288.

Schumann T, Paul S, Melzer M, Dörmann P, Jahns P. 2017. Plant growth under natural light conditions provides highly flexible short-term acclimation properties toward high light stress. *Frontiers in Plant Science* **8**: 681.

Schürmann P, Wolosiuk RA, Breazeale VD, Buchanan BB. 1976. Two proteins function in the regulation of photosynthetic CO_2 assimilation in chloroplasts. *Nature* **263**: 257–258.

Siefermann D, Yamamoto HY. 1975. Properties of NADPH and oxygen-dependent zeaxanthin epoxidation in isolated chloroplasts: a transmembrane model for the violaxanthin cycle. *Archives of Biochemistry and Biophysics* **171**: 70–77.

Stitt M, Lunn J, Usadel B. 2010. Arabidopsis and primary photosynthetic metabolism – more than the icing on the cake. *The Plant Journal* **61**: 1067–1091.

Takizawa K, Cruz JA, Kanazawa A, Kramer DM. 2007. The thylakoid proton motive force *in vivo*. Quantitative, non-invasive probes, energetics, and regulatory consequences of light-induced pmf. *Biochimica et Biophysica Acta* **1767**: 1233–1244.

Takizawa K, Kanazawa A, Kramer DM. 2008. Depletion of stromal P_i induces high 'energy-dependent' antenna exciton quenching (q_E) by decreasing proton conductivity at CF_0-CF_1 ATP synthase. *Plant, Cell & Environment* **31**: 235–243.

Thornber JP, Highkin HR. 1974. Composition of the photosynthetic apparatus of normal barley leaves and a mutant lacking chlorophyll b. *European Journal of Biochemistry* **41**: 109–116.

Tutkus M, Saccon F, Chmeliov J, Venckus O, Ciplys I, Ruban AV, Valkunas L. 2019. Single-molecule microscopy studies of LHCII enriched in Vio or Zea. *Biochimica et Biophysica Acta – Bioenergetics* **1860**: 499–507.

Uflewski M, Mielke S, Correa Galvis V, von Bismarck T, Chen X, Tietz E, Russ J, Luzarowski M, Sokolowska E, Skirycz A *et al.* 2021. Functional characterization of proton antiport regulation in the thylakoid membrane. *Plant Physiology* **187**: 2209–2229.

Van Kooten O, Snel JFH, Vredenberg WJ. 1986. Photosynthetic free energy transduction related to the electric potential changes across the thylakoid membrane. *Photosynthesis Research* **9**: 211–227.

Vialet-Chabrand S, Matthews JS, Simkin AJ, Raines CA, Lawson T. 2017. Importance of fluctuations in light on plant photosynthetic acclimation. *Plant Physiology* **173**: 2163–2179.

Vredenberg WJ. 1969. Light-induced changes in membrane potential of algal cells associated with photosynthetic electron transport. *Biochemical and Biophysical Research Communications* **37**: 785–792.

Walters RG, Horton P. 1994. Acclimation of *Arabidopsis thaliana* to the light environment: changes in composition of the photosynthetic apparatus. *Planta* **195**: 248–256.

Walters RG, Horton P. 1995. Acclimation of *Arabidopsis thaliana* to the light environment: regulation of chloroplast composition. *Planta* **197**: 475–481.

Wang C, Yamamoto H, Narumiya F, Munekage YN, Finazzi G, Szabo I, Shikanai T. 2017. Fine-tuned regulation of the K^+/H^+ antiporter KEA3 is required to optimize photosynthesis during induction. *The Plant Journal* **89**: 540–553.

Werdan K, Heldt HW, Milovancev M. 1975. The role of pH in the regulation of carbon fixation in the chloroplast stroma. Studies on CO_2 fixation in the light and dark. *Biochimica et Biophysica Acta* **396**: 276–292.

Xu P, Tian L, Kloz M, Croce R. 2015. Molecular insights into zeaxanthin-dependent quenching in higher plants. *Scientific Reports* **5**: 13679.

Supporting Information

Additional Supporting Information may be found online in the Supporting Information section at the end of the article.

Fig. S1 Light and climate of the different growth environments.

Fig. S2 PFD_{mean} and PFD_{var}-dependency of photosynthetic capacity and photoprotective pigments.

Fig. S3 Effects of growth conditions on thylakoid membrane composition.

Fig. S4 Effects of different growth environments on visual phenotypes and F_v/F_m of wild-type, *kea3*, and *vccn1*.

Fig. S5 Effects of different growth environments on nonphotochemical quenching and Φ_{PSII} of wild-type, *kea3*, and *vccn1* during light fluctuations.

Fig. S6 The effect of PFD_{mean} and PFD_{var} on nonphotochemical quenching and Φ_{PSII} of wild-type, *kea3*, and *vccn1* during light fluctuations.

Fig. S7 Validation of spectroscopic approach using mutants with defects in qE and Zx turnover.

Fig. S8 Characterization of nonphotochemical quenching using the IDEAspec, biomass, and KEA3 protein content under three selected growth conditions.

Fig. S9 Analysis of dynamic photosynthesis in *npq2* and *npq2 kea3-1* mutants.

Table S1 Light and climate of phytotron and polytunnel-grown plants.

Table S2 Deconvolution of spectroscopic data.

Table S3 Pigment content of thylakoid membranes.

Table S4 Thylakoid protein composition as determined by Western blotting.

Table S5 Thylakoid protein composition as determined by MS analysis.

Table S6 Effects of PFD_{mean} and PFD_{var} on photosynthetic factors.

Table S7 Effects of PFD_{mean} and PFD_{var} on thylakoid composition.

Table S8 Effects of PFD_{mean} and PFD_{var} on the *kea3* and *vccn1* nonphotochemical quenching phenotypes.

Table S9 Correlation analysis of Φ_{PSII}, nonphotochemical quenching, and CO_2 assimilation rate vs PFD_{mean} and PFD_{var} across genotypes and growth conditions.

Table S10 Correlation analysis of Φ_{PSII} vs nonphotochemical quenching across genotypes and growth conditions.

Table S11 Leaf pigments of wild-type and mutants from FD_L, FD_H, and DD_F.

Table S12 KEA3 content in wild-type, *kea3-1*, and *vccn1-1* from FD_L, FD_H, and DD_F.

Table S13 Deconvoluted qE_{535} traces during light fluctuations.

Table S14 Deconvoluted electrochromic shift traces during light fluctuations.

Table S15 Statistics on nonphotochemical quenching and Φ_{PSII} from wild-type, *kea3-1*, *npq2*, and *npq2 kea3-1*.

Please note: Wiley is not responsible for the content or functionality of any Supporting Information supplied by the authors. Any queries (other than missing material) should be directed to the *New Phytologist* Central Office.